5-2012

A Method for Performance Analysis of a Ramjet Engine in a Free-jet Test Facility and Analysis of Performance Uncertainty Contributors

Kevin Raymond Holst
kholst@utk.edu

To the Graduate Council:

I am submitting herewith a thesis written by Kevin Raymond Holst entitled "A Method for Performance Analysis of a Ramjet Engine in a Free-jet Test Facility and Analysis of Performance Uncertainty Contributors." I have examined the final electronic copy of this thesis for form and content and recommend that it be accepted in partial fulfillment of the requirements for the degree of Master of Science, with a major in Aerospace Engineering.

Basil N. Antar, Major Professor

We have read this thesis and recommend its acceptance:

Robert W. McAmis, Roy J. Schulz

Accepted for the Council:
Dixie L. Thompson

Vice Provost and Dean of the Graduate School

(Original signatures are on file with official student records.)

A Method for Performance Analysis of a Ramjet Engine in a Free-jet Test Facility and Analysis of Performance Uncertainty Contributors

A Thesis Presented for the

Master of Science

Degree

The University of Tennessee, Knoxville

Kevin Raymond Holst

May 2012

For Brian

ACKNOWLEDGEMENTS

I would like to express my heartfelt gratitude to the individuals that offered their knowledge and support during the preparation of this thesis. Dr. Rob McAmis guided me during my coursework at UTSI and helped push me to complete this thesis. Many hours were spent in his office in search of a thesis topic and a direction from which to approach it. The time he has devoted to helping me on this thesis, on my coursework, and through my career at AEDC is a testament to his high character and integrity. Dr. Doug Garrard at AEDC provided a task for me that was able to be spun into this thesis and offered his knowledge and expertise on the topic when needed. Mark Cross at AEDC made available his wealth of ground testing and uncertainty knowledge to help formulate this thesis. Dr. Roy Schulz offered a careful critique of this work which helped to clarify the topic and to give it additional technical depth. Dr. Basil Antar also provided a review of this proposal and graciously served as my thesis committee chair. Finally, I would like to acknowledge the patience and support of my wife, Kimberly. I will be forever grateful for her understanding of my desire to continue classes and complete this thesis, and her ability to help me retain my focus and positive outlook on the task.

ABSTRACT

Ramjet and scramjet engines are being developed to provide a more fuel efficient means of propulsion at high Mach numbers. Part of the development of these engines involves test and evaluation of an engine in ground facilities as well as in flight. Ground facilities, like Arnold Engineering Development Complex (AEDC) and those at engine manufacturers like General Electric (GE) and Pratt & Whitney (PW), have decades of experience testing traditional turbine engines and much less experience testing full scale ramjet engines.

Testing a supersonic engine in a free-jet mode presents a host of challenges not experienced during traditional direct connect turbine engine tests. Characterizing the performance of an engine in a free-jet test facility is a difficult task due in part to the difficulty in determining how much air the engine is ingesting and the spillage, friction and base drag of the engine installation.

As more exotic propulsion systems like DARPA's Falcon Combined Cycle Engine Test (FaCET) article or NASA's X-43 are developed, there is a greater need for effective ground tests to determine engine performance and operability prior to flight testing. This thesis proposes a method for calculating three key performance parameters (airflow, fuel flow, and thrust) and investigates the uncertainty influences for these calculations.

A data reduction method was developed for this thesis to calculate the engine airflow, net thrust, and specific impulse (I_{SP}) in a ground test of a generic ramjet engine in a free-jet test facility. It considered typical measurements for an engine test (pressures, temperatures, fuel flow, scale force, and engine and cowl geometry).

Once the code was developed, an uncertainty analysis of the calculations was conducted, starting with a simplified analytical assessment. A common industry accepted uncertainty approach was then used in conjunction with the data reduction code to determine the sensitivity or influence coefficients of the independent measurements on the dependent parameters by the dithering method. These influence coefficients were

used to ascertain where measurement improvements could be made to affect the greatest reduction in uncertainty of the predicted engine performance.

TABLE OF CONTENTS

LIST OF TABLES

LIST OF FIGURES

NOMENCLATURE

A	Cross-sectional area	in^2
A_0	Inlet capture stream tube area	in^2
A_6	Nozzle exit area	in^2
A_{6eff}	Nozzle exit effective area	in^2
A_{AS}	Aft test stand area	in^2
A_{FS}	Forward test stand area	in^2
A^*	Sonic venturi nozzle throat area	in^2
b	Systematic standard uncertainty	%
C_d	Venturi nozzle discharge coefficient	
C_R	Venturi nozzle real gas critical flow coefficient	
D_{fm}	Flowmeter inlet diameter	in
D_{fmcal}	Flowmeter inlet diameter at calibration	in
d_{th}	Venturi nozzle throat diameter	in
E	Modulus of elasticity	psi
F_{drag}	Drag force	lbf
F_{meas}	Measured scale force	lbf
F_{measC}	Measured scale force (cold flow)	lbf
F_{net}	Calculated net thrust	lbf
F_{netC}	Calculated net thrust (cold flow)	lbf
f	Frequency	hz
g_0	Gravitational acceleration at sea level	ft/s^2
I_{SP}	Fuel specific impulse	s
K	Flowmeter K-factor	$hz/(ft^3/s)$
M	Mach number	
M_0	Inlet Mach number	
M_{0c}	Inlet Mach number (cold flow)	
$\dot{m}$	Air mass flow rate	lbm/s

$\dot{m}_{fuel}$	Fuel mass flow rate	lbm/s
N	Number of samples taken for $\bar{X}$	
P	Static pressure	psia
P_0	Inlet cell pressure	psia
P_6	Nozzle exit static pressure	psia
P_{amb}	Ambient test cell static pressure	psia
P_{AS}	Aft test stand pressure	psia
P_{ASC}	Aft test stand pressure (cold flow)	psia
P_{FS}	Forward test stand pressure	psia
P_{FSC}	Forward test stand pressure (cold flow)	psia
P_{fuel}	Fuel pressure	psia
$P_{fuelcal}$	Fuel pressure at calibration	psia
P_t	Total pressure	psia
P_{t0}	Inlet total pressure	psia
P_{t0c}	Inlet total pressure (cold flow)	psia
P_{t5}	Nozzle throat total pressure	psia
P_{tv}	Venturi nozzle throat total pressure	psia
P^*	Sonic venturi nozzle throat static pressure	psia
R	Gas constant or calculation result for calculation uncertainty description	(ft*lbf)/(sl*°R)
Re	Reynolds number	
Ro	Roshko number	
Sa_0	Inlet stream thrust	lbf
Sa_{6I}	Ideal nozzle stream thrust	lbf
St	Strouhal number	
s	Random standard uncertainty	%
T	Static temperature	°R
T_{fuel}	Fuel temperature	°R
$T_{fuelcal}$	Fuel temperature at calibration	°R
T_t	Total temperature	°R

T_{t0}	Inlet total temperature	°R
T_{t0c}	Inlet total temperature (cold flow)	°R
T_{t5}	Nozzle throat total temperature	°R
T_{tv}	Venturi nozzle throat total temperature	°R
t_{fm}	Flowmeter wall thickness	in
U	Combined total uncertainty	%
u	Combined standard uncertainty	%
V	Velocity	ft/s
V_0	Inlet velocity	ft/s
V_6	Nozzle exit velocity	ft/s
V^*	Sonic venturi nozzle throat velocity	ft/s
$\dot{V}$	Volumetric flow rate	ft^3/s
X	individual observation of a parameter in a data sample	
$\bar{X}$	Sample mean; average of a set of N individual observations of a parameter	*
	Greek Characters	
α	Coefficient of linear thermal expansion	$°R^{-1}$
β	Systematic error	*
γ	Ratio of specific heats	
ε	Random error	*
η_{noz}	Nozzle stream thrust efficiency	
θ	Absolute influence coefficient	*
θ'	Relative influence coefficient	
μ	Population mean	*
ν	Kinematic viscosity	cSt
ρ	Density	lbm/ft^3
ρ_{fuel}	Fuel density	lbm/ft^3

CHAPTER I

INTRODUCTION AND PROBLEM STATEMENT

Ground Test Facilities

In modern propulsion systems, adequate ground testing requires accurate simulation of flight conditions that the engine would be subjected to during normal operations. Large scale altitude test facilities, like the United States Air Force's Arnold Engineering Development Complex (AEDC) and formerly the Royal Aircraft Establishment's National Gas Turbine Establishment (NGTE Pyestock), along with corporately owned, sea-level test facilities were developed to meet the experimental needs for accurate simulations.

For hypersonic systems, a variety of test facilities exist, from shock tubes, where tests are limited to milliseconds, to continuous flow wind tunnels. The purpose of all types of aeropropulsion test facilities is to simulate the conditions a test article would see in flight. Some of the typical conditions simulated include inlet pressure, temperature, mass flow, air chemistry, and exhaust (or ambient) pressure. Others like inlet pressure and temperature distortion and icing can also be simulated, if required. The combination of all of these conditions will reproduce the desired test Mach number and altitude, or for some test cases the desired dynamic pressure and enthalpy. Due to the high mass flows required, high pressures and temperatures must be provided by the supply systems of continuous flow facilities, which typically makes test costs prohibitive. Blow-down facilities are usually more economical but can only provide air flow on test conditions for a relatively short amount of time (usually, on the order of a few minutes).

A typical combustion-vitiated blow-down facility operates by storing a large quantity of high pressure air in tanks prior to a test. This air is then fed into a combustor chamber where fuel and oxygen are added to heat up the air to the correct total temperature, while still maintaining the desired amount of oxygen in the flow supplied to the test article. The high temperature, high pressure vitiated air then flows through a

nozzle that accelerates the flow to a desired Mach number within the test cell where it is collected by the inlet of the test article.

Engine test facilities must also be able to reproduce the simulated flight conditions for numerous repeated tests with a high degree of accuracy. The repeatability is very important to the measurement of engine air flow, because a standard way to measure the air flow captured by an engine is to replace a section of the engine, aft of the inlet and isolator, with an air flow calibration device. Typically experiments are run with the calibration device installed to the establish inlet mass capture ratio, followed by testing of the full engine.

Ramjet and Scramjet Background

Ramjets and scramjets are two types of air breathing propulsion systems that, unlike turbojets and turbofans, do not employ rotating turbomachinery to compress inlet air prior to fuel addition and combustion; rather, they compress the incoming air through supersonic inlets and diffusers, with compression due to complex shock structures in the flow. Because they rely solely on this form of compression, they are only able to operate at flight speeds well in excess of the local speed of sound. Currently high Mach number (approximately greater than Mach number of 3.5) sustained flight can only reliably be achieved using rockets. The lure of ramjets and scramjets is that they offer high Mach number flight also, but without the need to carry oxidizer onboard the flight vehicle. This results in a higher specific impulse, I_{SP}, which is a general measure of system efficiency. Equation (1-1) defines air-breathing engine I_{SP}. Figure 1 shows a notional chart of I_{SP} versus Mach number for air breathing propulsion systems and rockets, with some actual engine data plotted on it for perspective. It shows that as Mach number increases through approximately 3.0, engines with rotating turbomachinery become much less efficient than ramjets. Ramjets then see a similar drop off in efficiency at Mach 5.8, giving way to more efficient scramjets.

$$I_{SP} = \frac{F_{net}}{\dot{m}_{fuel} * g_0} \tag{1-1}$$

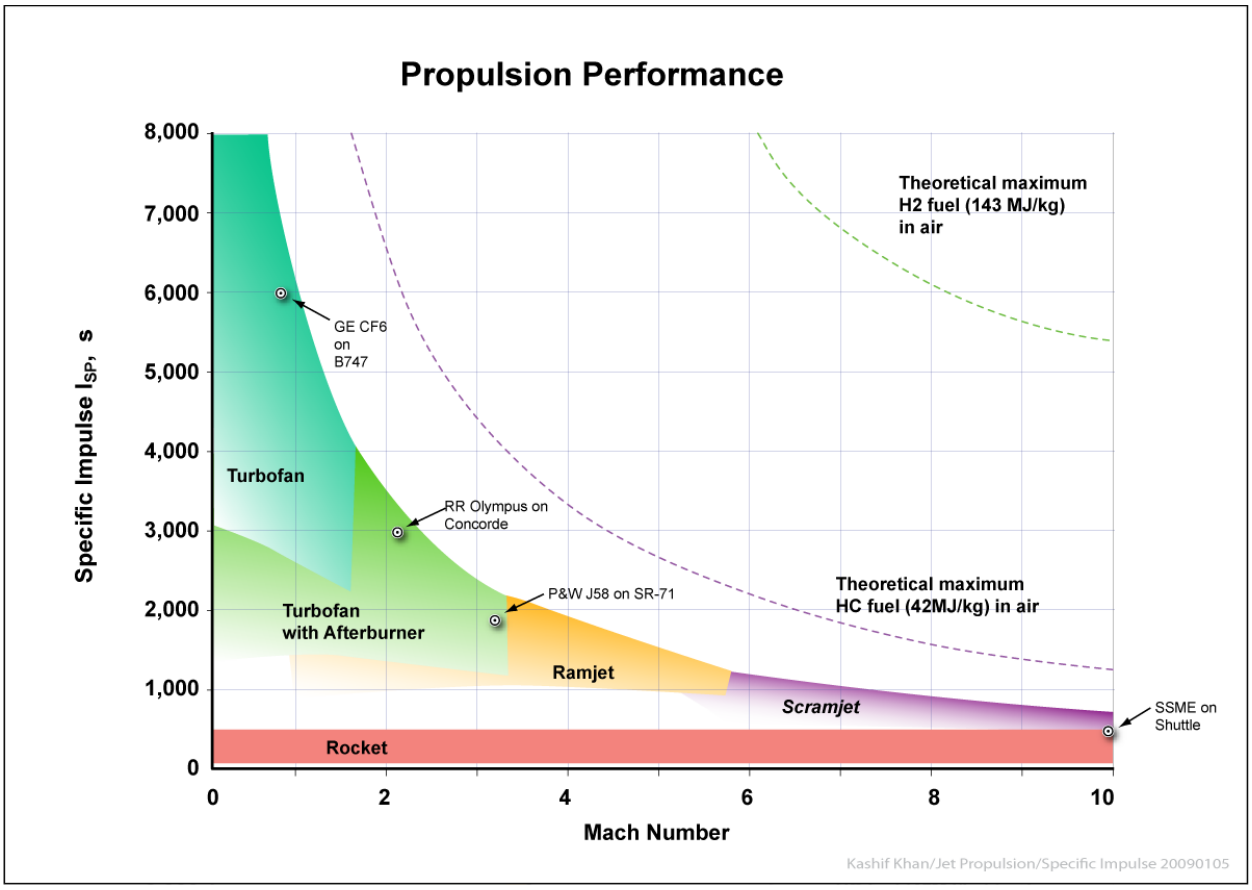

Figure 1: Air breathing and rocket propulsion comparison

In a typical ramjet engine (shown in Figure 2), supersonic air is ingested by the inlet diffuser and compressed through a series of oblique shocks followed by a normal shock, which brings the airflow to a subsonic velocity prior to reaching the combustor. The flow is typically decelerated even more using a divergent duct just prior to entering the combustor. Fuel is then injected in the combustor where it mixes with the subsonic air and burns to add energy to the airflow. The burned air-fuel mixture is then ejected through a converging-diverging nozzle where it is accelerated to a supersonic velocity out the aft end of the engine. (Heiser & Pratt, 1994)

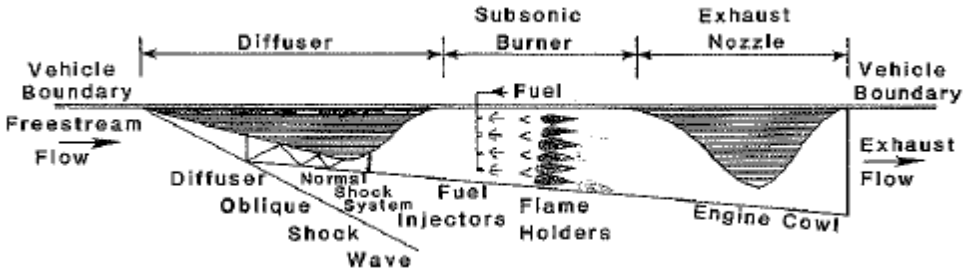

Figure 2: A typical two-dimensional ramjet engine

A typical scramjet engine (displayed in Figure 3) has some key differences. The supersonic/hypersonic air is ingested by the inlet diffuser and is compressed through a series of oblique shocks. The airflow then travels through a constant area diffuser called an isolator, where it continues to be compressed through oblique shocks. The isolator acts as a barrier between the inlet and pressure disturbances in the combustor section in order to prevent inlet unstart, which occurs when the pressure in the combustor gets so high that it stops the flow into the inlet by breaking down the inlet shock system. The air maintains supersonic velocity out of the isolator and enters the combustor where fuel is added, mixed, and then burned. In the combustor of a scramjet, it is important not to add too much energy to the flow because a thermal throat can form, causing the flow to go subsonic. After the combustor, the air is then accelerated through a diverging nozzle out the aft end of the engine. The key difference between a ramjet and a scramjet is that the flow through a scramjet engine can never be fully subsonic at some station of the flow path. (Heiser & Pratt, 1994)

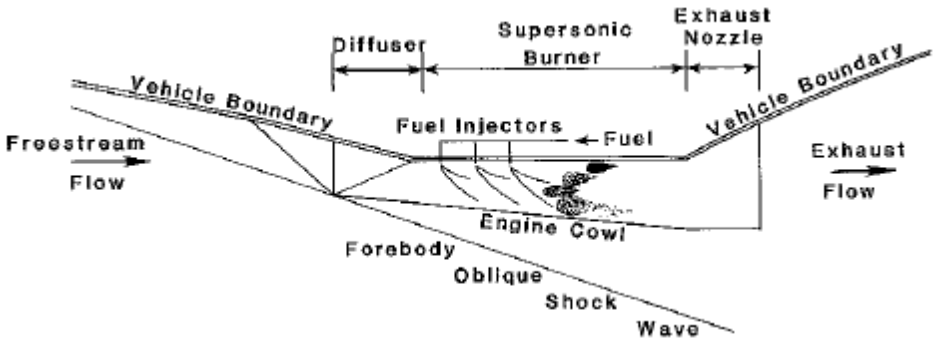

Figure 3: A typical two-dimensional scramjet engine

A dual-mode ramjet (DMR) may function as either a ramjet or a scramjet, depending on the flight Mach number. This can be achieved with a fixed geometry and a thermal throat if the range of operating Mach numbers is not too wide; however, if a larger Mach number range is required, variable geometry inlets or combustors may be required. (Falempin, 2008)

Free-jet Testing Compared to Direct Connect Testing

For typical modern turbine engines, simulated altitude testing is conducted using a direct-connect set up, shown in Figure 4. (Smith V. K.) During this type of test, an engine is placed in a test cell that is used to simulate flight conditions (altitude and Mach number). An air supply facility is connected to the engine compressor face inlet by a duct. Exhaust from the engine nozzle flows into the test cell and is pumped out through an exhaust facility diffuser and exhaust duct. The air supply and exhaust facilities work in conjunction to simulate flight conditions. The air supply provides air to the compressor face or isolator inlet at a desired total pressure and total temperature that represent flow conditions downstream of the airframe inlet or supersonic inlet, and the exhaust facility pumps the test cell to a desired static pressure.

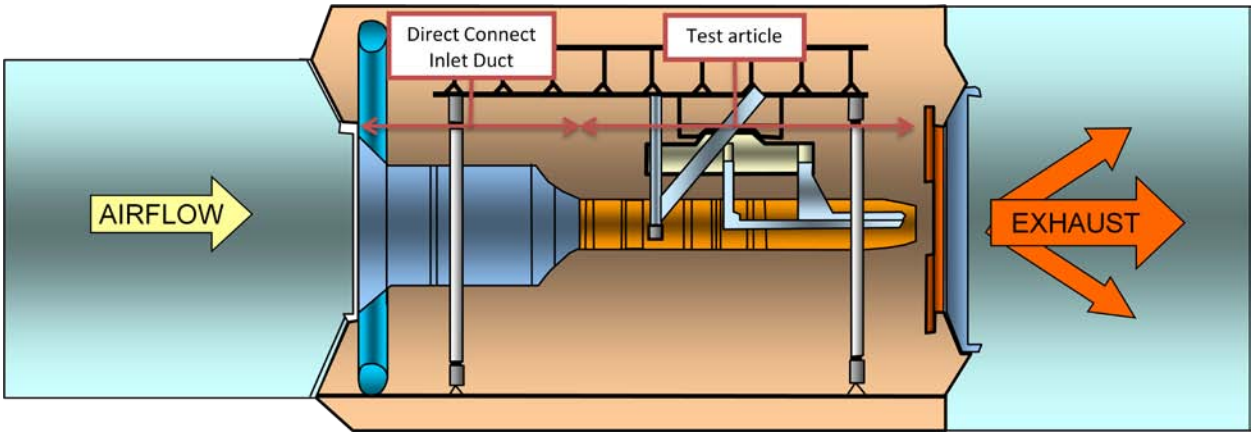

Figure 4: Direct connect configuration

Complete ramjet and scramjet engine systems are typically tested in free-jet test cells, like the Aerodynamic and Propulsion Test Unit (APTU) shown in Figure 5. (Dunsworth & Reed)(Falempin, 2008)(Smith V. K.)(Goyne, Crisci, & Fetterhoff, 2009)(Smart & Ruf, 2006)(Voland, Auslender, Smart, Roudakov, Semenov, & Kopchenov, 1999) These differ from direct connect only on the air supply side. Rather than being directly connected to the air supply with a duct attached directly to the compressor or isolator inlet, a free-jet test cell provides a large supply of air into the cell itself through a free-jet nozzle and the airframe or engine inlet captures the air as it would in flight. In a high Mach number free-jet test, high pressure and high temperature air must be supplied to the test article at mass flow rates that may reach up to 230 pound-mass per second per square foot of flow area. (Dunsworth & Reed)

As mentioned previously, there are two major types of facilities used for full ramjet and scramjet system testing: blow-down and continuous flow. They differ on how the inlet air is supplied to the free-jet nozzle and subsequently to the test article. In a blow-down facility, all of the air for a test is pressurized and stored prior to the test, typically in numerous large high pressure storage bottles. Once initiated all of the stored air flows through pressure regulators and burners or indirect heaters before coming to the free-jet nozzle, where it is accelerated to desired Mach number and introduced into the test cell where the test article resides. This type of test can only be conducted for a specific amount of time depending on the amount of air stored and the mass flow rate

required for test article at the desired flight conditions. In contrast a continuous flow test facility uses compressors and air heaters, if necessary, to provide uninterrupted conditioned flow to the free-jet nozzle. Due to the high mass flows required at high pressures and temperatures, blow-down facilities are typically the most economic solution to obtaining engine performance data. (Dunsworth & Reed)

There are a variety of methods for achieving the high air supply temperatures required. A typical vitiation-type combustion air heater (CAH) employs a combustor upstream of the free-jet nozzle and injects additional oxygen to compensate for the oxygen consumed in the combustion process. This produces vitiated air flow that has the correct amount of oxygen, but has a higher amount of combustion products, like water and carbon dioxide, than clean air. Methods of providing clean, high temperature air exist (such as pebble bed storage heaters), but they also have their drawbacks, not the least of which is the significant amount of time required to bring the heat storage material up to temperature prior to testing. It is important to note that vitiated air has been proven to have an insignificant effect on ramjet engine testing (Dunsworth & Reed), but the effects of vitiation on scramjet engine testing are still being gathered and analyzed (Fetterhoff, Bancroft, Burfitt, Osborne, Hawkins, & Schulz, 2011).

Although component testing can be conducted in a direct connect test cell, full ramjet and scramjet engines are tested in free-jet test cells to capture the actual behavior of their inlet diffusers as they compress the incoming air. They require freestream air flow in order for the designed shock structure to form at the engine inlet. Typically a specific free-jet nozzle will be used to simulate a specific flight Mach number; variable Mach number free-jet nozzles are currently in development.

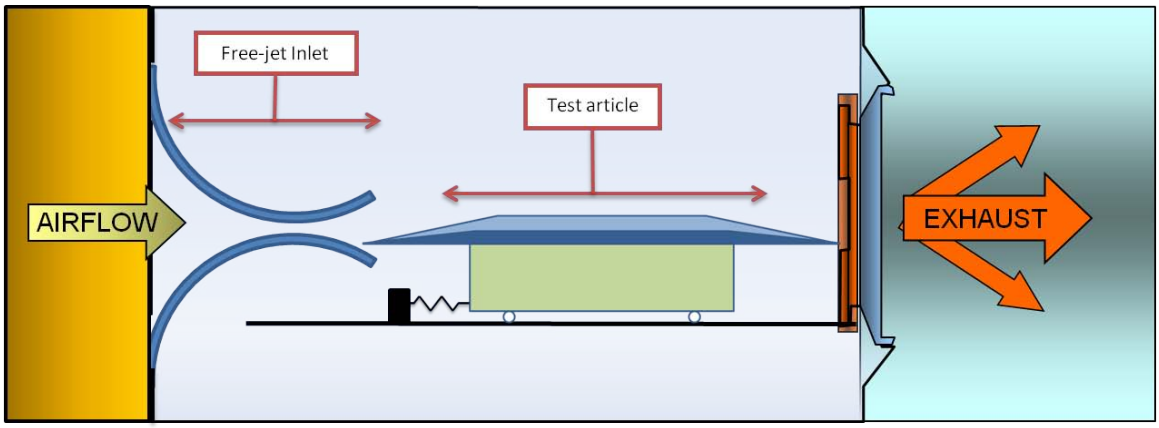

Figure 5: Typical free-jet test cell

Instrumentation

Ramjet testing requires minimally intrusive instrumentation due to the supersonic/hypersonic airflow in the inlet. By intrusive, it is meant that the instrumentation would extend into the flow stream, causing extra, undesirable shockwaves and pressure losses in the flow. A typical turbofan engine for subsonic flow may be outfitted with total pressure and temperature rakes that protrude into the airflow at various stations throughout the engine. This would not be acceptable in a ramjet because of the larger effects the rake would have on the airflow, whether that be due to the induction of additional turbulence or the creation of unintended shock structures in supersonic flow. As a result of this limitation the majority of instrumentation on a ramjet test article are static pressures, skin temperatures, and heat flux gages. Other instrumentation that would be used on a typical free-jet engine test includes:

- Load cells to measure the force exerted on the engine support structure
- Fuel flowmeters to measure the amount of fuel being delivered to the combustor
- External static pressure taps on the support structure to calculate the pressure forces on the support structure
- Total pressure and temperature probes close to, but not in front of, the inlet to determine the conditions of the incoming air

Data Analysis

Once a test has been conducted, the measured data are analyzed to determine the performance of the engine in terms of calculations of air flow, net thrust, specific impulse (I_{SP}), and any other metrics of interest. These calculations allow the engineer to compare the performance of one engine, to another engine, to predicted design goals, or to engine specifications.

An important additional part of this analysis is the estimation of the uncertainty in the performance calculations. Every measurement has an inherent error in it that can be defined as the difference between the measurement and the "true" value. The exact value of the error is unknown, but the range that it will likely lie between can be estimated. This estimate is called the uncertainty of the measurement. Measurement uncertainties propagate into the calculated values of airflow, net thrust, and I_{SP}, and estimates for the resulting uncertainties of the performance calculations should be included whenever an experiment is conducted.

The propagation of uncertainties into calculated parameters is accomplished by weighting the uncertainty of each component of the calculation according to its influence on the calculation. The influence of each component can be computed a number of different ways. The complex sets of equations that will be used to calculate the performance parameters in the data reduction computer code make analytical methods of data reduction very tedious and time prohibitive. The performance equations, however, can often be simplified for uncertainty analysis and error propagation. That being said, since a computer program is almost always written to perform data reduction calculations, the same numerical program can be utilized to perform uncertainty calculations and error propagation. The typical numerical methods for calculating uncertainty are dithering and Monte Carlo (Dieck, 1997). The uncertainty program used for this thesis will employ the dithering method to determine the influence coefficients of the independent measurements on the dependent calculations.

By understanding how performance metrics are calculated and the corresponding uncertainty with their calculations, a valid comparison between engine systems can be made. Values for performance metrics alone, especially those of state-of-the-art engines

that are tested in unique facilities, do not provide enough information for a valid comparison to be made; uncertainties are also greatly needed.

Problem Statement

The objective of this thesis is to create a data reduction process to compute engine performance metrics of air flow, net thrust, and I_{SP} and to estimate the uncertainty of these metrics from a free-jet test of a generic ramjet engine. The uncertainties on the performance parameters are calculated analytically using simplified equations and numerically using the dithering method, which employs the data reduction process to determine the sensitivity coefficients of measurements on the performance calculations. The steps taken in this thesis to assess overall ramjet engine performance uncertainty influence factors follow the general method outlined by Smith, et al (Smith, Scheid, Eklund, Gruber, Wilkin, & Mathur, 2008) for a supersonic combustion research laboratory, but the steps are tailored to apply to the ramjet engine test process (free-jet testing) chosen for analysis.

The analysis for this thesis was conducted assuming an ideal ground free-jet ground test of a ramjet engine. This assumes the free-jet nozzle is large enough to provide uniform, parallel airflow into the test cell, the test article is ideally situated within the free-jet airflow to receive the required amount of airflow at the desired conditions, and the chemical properties of the free-jet airflow are uniform and known.

CHAPTER II

LITERATURE REVIEW

Ramjet Performance Analysis

The focus of this thesis is on the calculation of airflow, net thrust, and I_{SP}. Many other measures of performance exist, such as diffuser pressure ratio, propulsive efficiency, and combustion efficiency, but they have been ignored to simplify the problem.

Uncertainty

Many sources were investigated to guide the uncertainty analysis for this thesis (Coleman & Steele, 1999) (Dieck, 1997)(Evaluation of measurement data - Guide to the expression of uncertainty in measurement, 2008)(Guidelines for Evaluating and Expressing the Uncertainty of NIST Measurement Results, 1994)(Test Uncertainty, 2006); however, ASME PTC-19.1-2005 *Test Uncertainty* (Test Uncertainty, 2006) was chosen as the reference to follow. PTC-19.1 was designed to follow the International Organization for Standardization (ISO) *Evaluation of measurement data – Guide to the expression of uncertainty in measurement* (GUM) (Evaluation of measurement data - Guide to the expression of uncertainty in measurement, 2008), because it provides a more concise and practical guide for an engineer than the GUM. This is accomplished in PTC-19.1 by placing more emphasis on the effect that errors have on measurements and calculations and less emphasis on the origin of the information used to approximate their limits.

Measurement Uncertainty

Engine ground tests are conducted with the goal of determining how an engine operates in terms of its performance, operability, stall margin, and a variety of other metrics. Measurements (pressure, temperature, airflow, fuel flow, and force

measurements, among others) are made to evaluate these metrics, and often the measured values are compared to predicted values provided by engine cycle models.

The *International Vocabulary of Metrology* (VIM) (International vocabulary of metrology - Basic and general concepts and associated terms, 2008) defines measurement as a "process of experimentally obtaining one or more quantity values that can reasonably be attributed to a quantity." Each value of a parameter or quantity obtained through measurement is an approximation of the true value of the quantity being measured. The difference between the true and measured values is the total error. The total error of a measurement is not known; rather, its limits are estimated through analysis of its elemental components. These limits determine a coverage interval around the measured value where the true value is believed to lie, with a defined level of confidence (usually 95%). This coverage interval is also known as the total measurement uncertainty.

The total measurement error is comprised of two types of elemental error sources: random and systematic. Random error, ε, is the component of the total measurement error that varies unpredictably, or randomly, with each measurement. Systematic errors, β, are those that either remain constant over multiple measurements or vary in a predictable manner. The total measurement uncertainty is the linear combination of uncertainties due to both random and systematic errors. Figure 6 shows a graphical depiction of the statistical distribution of measured values of a variable with a large enough number of samples to be accurately fit by an appropriate statistical distribution function. The random and systematic components of total measurement error are depicted on the figure. (Test Uncertainty, 2006) The GUM and PTC-19.1 further distinguish the components of the total measurement uncertainty as "Type A" or "Type B." These labels are used to indicate how particular elemental uncertainties are given their measure. "Type A" uncertainties result from using statistical analyses of measurements. "Type B" uncertainties are simply those that do not come from statistical analyses; they may come from "engineering judgment," for example.

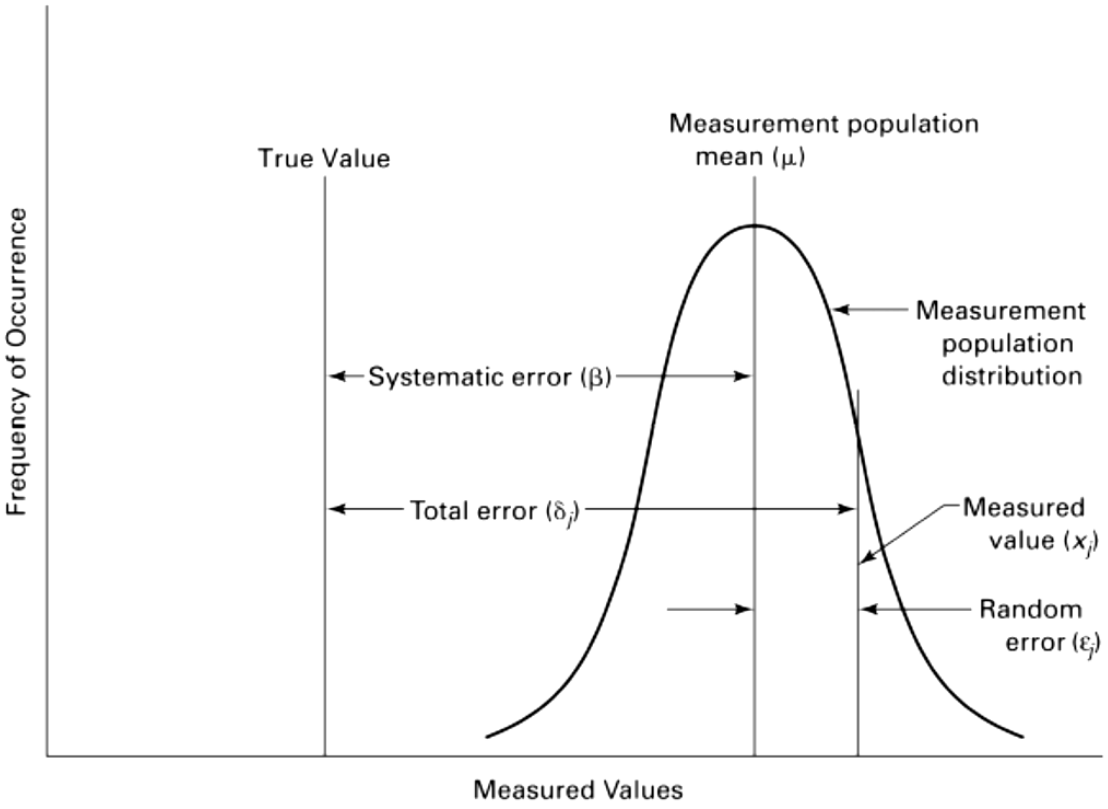

Figure 6: Graphical depiction of measurement errors for a normally-distributed variable (a Gaussian variable)

The measurement population mean, μ, and the measurement population distribution in Figure 6 assume that the population used to describe them is infinite. Only a finite number of measurements are acquired during a test, and as a result sample statistics must be used to estimate the population mean and standard deviation. The sample mean and sample standard deviation are shown in Eqs. (2-1) and (2-2), respectively.

$$\bar{X} = \frac{\sum_{j=1}^{N} X_j}{N} \tag{2-1}$$

$$s_{\bar{X}} = \frac{s_X}{\sqrt{N}} = \sqrt{\sum_{j=1}^{N} \frac{\left(X_j - \bar{X}\right)^2}{N(N-1)}} \tag{2-2}$$

The measurement uncertainty is determined through separate examination of the random and systematic error sources. Random and systematic errors result from numerous individual error sources that must be accounted for. The elemental uncertainties of the individual random error sources are combined using the root-sum-squared (RSS) method according to Eq. (2-3) to form the random standard uncertainty for the measurement mean, $s_{\bar{X}}$.

$$s_{\bar{X}} = \sqrt{\sum_{k=1}^{K} {s_{\bar{X}_k}}^2} \tag{2-3}$$

Where K is the number of independent random error sources, such as calibration or environmental effects. The elemental uncertainties of the individual systematic error sources are similarly combined using the RSS method, as seen in Eq. (2-4).

$$b_{\bar{X}} = \sqrt{\sum_{k=1}^{K} {b_{\bar{X}_k}}^2} \tag{2-4}$$

The random and systematic standard uncertainties are then combined using the RSS method to form the combined standard uncertainty, Eq. (2-5).

$$u_{\bar{X}} = \sqrt{{b_{\bar{X}}}^2 + {s_{\bar{X}}}^2} \tag{2-5}$$

For large sample sets, the combined standard uncertainty is analogous to an estimate of the standard deviation of the total measurement error. The combined standard uncertainty is multiplied by an expansion factor, based on Student's t-distribution, to specify a coverage interval at a desired confidence level. Most engineering applications assume a large number (>30) of degrees of freedom and use an expansion factor of 2 to represent uncertainties at 95% confidence. The total measurement uncertainty, $U_{\bar{X}}$, for 95% confidence is calculated in Eq. (2-6).

$$U_{\bar{X}} = 2u_{\bar{X}} \tag{2-6}$$

A measurement, $\bar{X}$, with its corresponding uncertainty, $U_{\bar{X}}$, is typically expressed as:

$$\bar{X} \pm U_{\bar{X}} \tag{2-7}$$

It is important to note that the measurement uncertainty calculations in this section were absolute, meaning they retained the units of the measurement being conducted.

Calculation Uncertainty

Most of the engine performance metrics of interest are calculated from measurements of pressures, temperatures, flow rates, and other engine variables as well as other unmeasured quantities such as physical constants of the flow passing through and around the engine like the ratio of specific heats, γ. The uncertainties of all of the components in the calculated metric must be known or estimated in order to determine the uncertainty in the calculated parameter. The uncertainties of these measured and unmeasured components must be propagated into the calculation with sensitivity (or influence) coefficients that utilize the functional relationship between the calculation and the input components.

Sensitivity coefficients are a measure of how much influence each parameter has on the final calculated value of the metric. These can be absolute (dimensional, θ_i) or relative (non-dimensional, θ'_i) and can be computed analytically or numerically. The equations for analytically computing the absolute and relative sensitivity coefficients of a measurement, $\bar{X}_i$, on a calculation result, R, are shown in Eqs. (2-8) and (2-9), respectively.

$$\theta_i = \frac{\partial R}{\partial \bar{X}_i} \tag{2-8}$$

$$\theta'_i = \frac{\bar{X}_i}{R}\left(\frac{\partial R}{\partial \bar{X}_i}\right) \tag{2-9}$$

The numerical estimation of the sensitivity coefficients is nearly identical to the analytical value, with numerical partial derivatives replacing the definite derivatives.

With the sensitivity coefficients calculated, calculation uncertainty is computed similarly to measurement uncertainty. The random and systematic standard uncertainties for each parameter in the calculation are segregated and then combined using the RSS method, with the sensitivity coefficients, to form the random and systematic standard

uncertainties for the calculation (Eqs. (2-10a,b) and (2-11a,b)). The random and systematic standard uncertainties for the calculation are then combined via RSS to form the calculation standard uncertainty (Eq. (2-12)). This is then combined with the expansion factor based on the desired coverage interval to determine the total calculation uncertainty.

$$s_R = \sqrt{\sum_{i=1}^{I} \left(\theta_i s_{\bar{X}_i}\right)^2} \tag{2-10a}$$

$$\frac{s_R}{R} = \sqrt{\sum_{i=1}^{I} \left(\theta'_i \frac{s_{\bar{X}_i}}{\bar{X}_i}\right)^2} \tag{2-10b}$$

$$b_R = \sqrt{\sum_{i=1}^{I} \left(\theta_i b_{\bar{X}_i}\right)^2} \tag{2-11a}$$

$$\frac{b_R}{R} = \sqrt{\sum_{i=1}^{I} \left(\theta'_i \frac{b_{\bar{X}_i}}{\bar{X}_i}\right)^2} \tag{2-11b}$$

$$u_R = \sqrt{{b_R}^2 + {s_R}^2} \tag{2-12}$$

Standardization of Ramjet Performance Reporting

The Chemical Propulsion Information Agency (CPIA), sponsored by Johns Hopkins University Applied Physics Lab (JHU/APL), published a report in March 1976 (McVey, 1976) aimed at standardizing the reporting of ramjet performance in an effort to reduce complications in correlating non-standard data. This report defined the engine station numbering system (shown in Figure 7), test data reporting requirements for each test point, and the associated performance data that should be calculated and reported. This report also defined standard calculations for specific performance parameters, to prevent different calculations being performed to come up with the same performance parameter. This would allow data to be compared more easily between separate engine

tests. The engine station numbering from this suggested standard has been followed in this thesis.

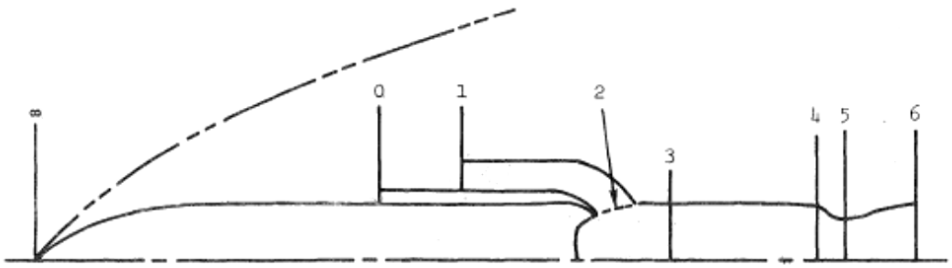

STATION NO.	DESCRIPTION - LOCATION
∞	Freestream
0	Vehicle flow field immediately upstream of the air induction system
1	Capture station - Beginning of internal flow system
2	Diffuser Exit
3	Combustor Entrance
4	Combustor Exit
5	Exhaust nozzle geometric throat
6	Nozzle Exit

Figure 7: Ramjet engine station descriptions from CPIA 276

CHAPTER III

APPROACH

Outline

The following is an outline of the intended approach to calculate ramjet engine performance and evaluate the uncertainty of those calculations using both an analytical approach and a numerical approach.

1. Create and check out a data reduction and engine performance prediction (DREPP) program to examine air flow, net thrust, and I_{SP} for a typical ramjet engine.
2. Use a simplified version of the data reduction equations to analytically estimate the influence coefficients of the desired performance parameters.
3. Numerically estimate the influence coefficients of the desired predicted engine performance parameters using DREPP.
4. Compare the influence coefficients obtained using analytical and numerical methods.
5. Identify where increased measurement accuracy would show greatest reduction in engine performance uncertainty.

Data Reduction

Data reduction is the process of using engineering unit (EU) measurement data from an experiment, like static pressures or force measurements, to calculate performance parameters. Typical methods for data reduction involve a data reduction computer code that accepts EU inputs and outputs the desired calculations. This can be done using anything from a sophisticated online data reduction system to provide real-time or near real-time data reduction to a simple spreadsheet used post-test. Using a computer program for data reduction also enables sensitivity coefficients to be easily determined from the dithering method.

Engine Airflow

One of the most significant difficulties with free-jet testing is accurately measuring and calculating the engine airflow. The engine airflow value propagates into

many other performance parameters such as thrust and specific impulse, and as a result, it is a very important parameter to know accurately. Unlike in a direct connect test, where all of the air being provided to the test cell is measured prior to passing through a duct and directly into an engine inlet, a free-jet test supplies an amount of air much larger than what the engine requires, and the engine inlet only takes in the portion of air that it needs.

Generally airflow is measured in a free-jet test by replacing a section of the engine aft of the inlet with an airflow measurement device (Figure 8). The test profile is run with the measurement device in place without the engine running, and airflow is calculated at points of interest through the run. Once the airflow measurement run, or cold flow run, is completed, the inlet capture stream tube cross-sectional area is calculated and the measurement device is removed from the engine and replaced by the previously removed aft section of the engine. The test profile is run again for a performance run. It is important that the performance run be conducted as similarly as possible to the airflow measurement run.

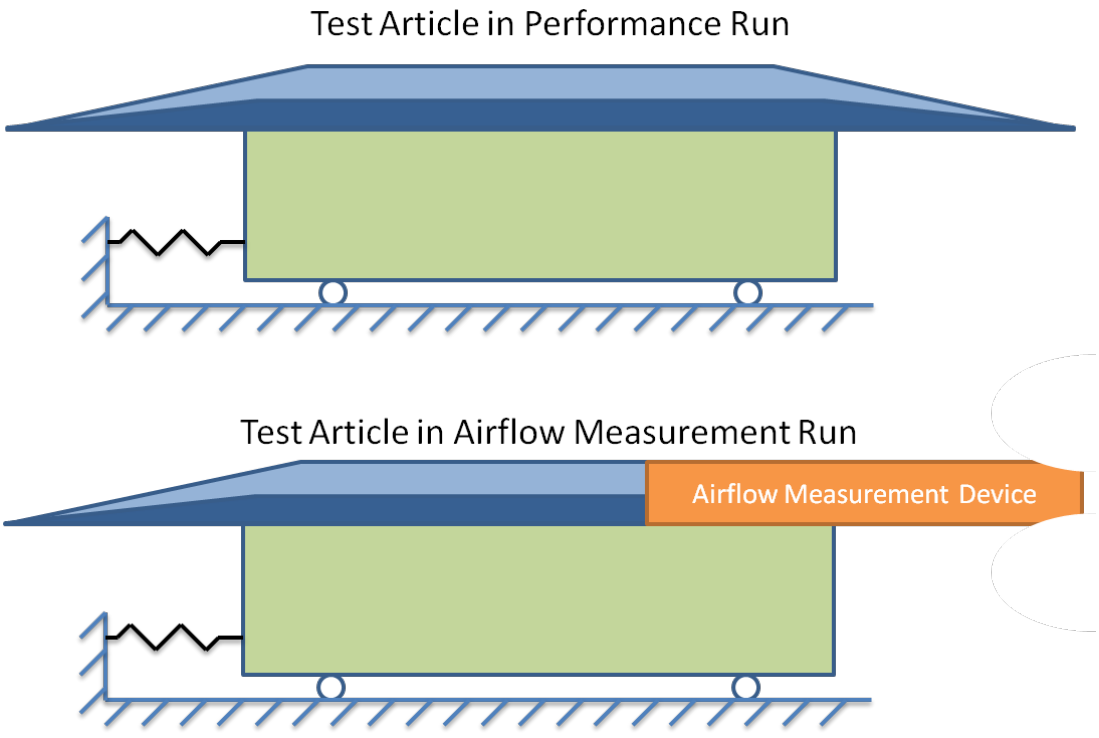

Figure 8: Illustration of airflow measurement device installation location on test article

This thesis describes the use of a critical flow toroidal venturi nozzle (Figure 9) to measure mass flow in accordance with ASME MFC-7M-1987 (Measurement of Gas Flow by Means of Critical Flow Venturi Nozzles, 1987) recommendations. A critical flow venturi nozzle is one whose throat area is small enough that the flow chokes at the test conditions. Choked flow in the throat of the venturi nozzle means that the airflow at the throat is at sonic velocity, or Mach 1. This is a desirable condition because only the total pressure and temperature upstream of the venturi throat are required to make the airflow calculation. The static pressure and static temperature at the venturi throat can be calculated using isentropic compressible flow equations (Eq. (3-1) and (3-2)).

$$P = P_t \left(1 + \frac{\gamma - 1}{2} M^2\right)^{\frac{\gamma}{1-\gamma}} \tag{3-1}$$

$$T = T_t \left(1 + \frac{\gamma - 1}{2} M^2\right)^{-1} \tag{3-2}$$

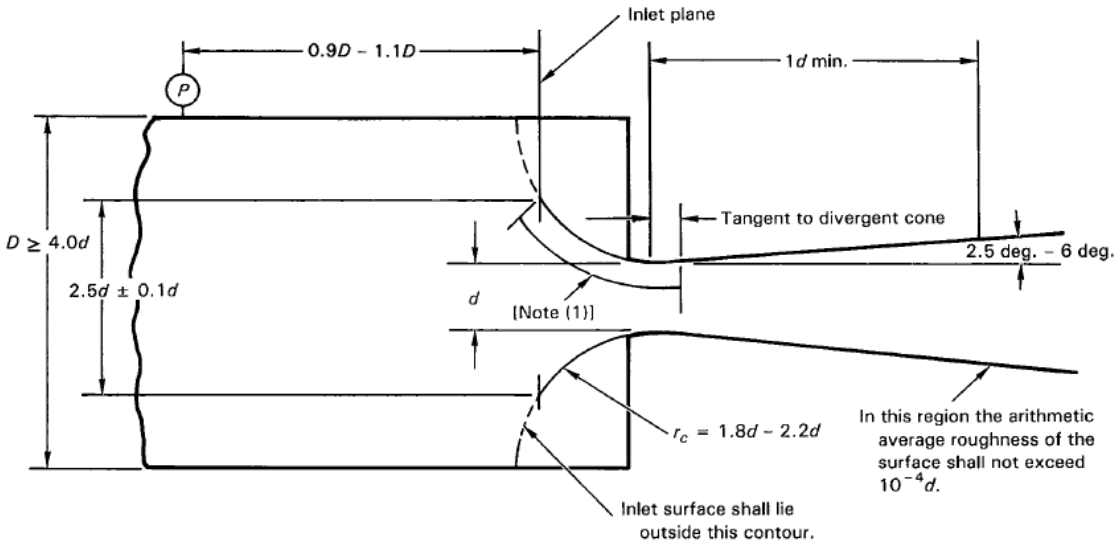

NOTE:
(1) In this region the surface shall not exceed $15 \times 10^{-6}d$ arithmetic average roughness and the contour shall not deviate from toroidal form by more than $0.001d$.

Figure 9: Toroidal throat venturi nozzle specification

MFC-7M-1987 provides a method for calculating mass flow through the venturi nozzle. The general equation for mass flow is given in Eq. (3-3).

$$\dot{m} = A^* C_d C_R P_t / \sqrt{R T_t} \quad (3\text{-}3)$$

The discharge coefficient, C_d, can be estimated from the following equation, given in MFC-7M-1987:

$$C_d = a - b * {Re_{dth}}^{-n} \quad (3\text{-}4)$$

Where, for a toroidal venturi nozzle:

$$a = 0.9935$$

$$b = 1.525$$

$$n = 0.5$$

This discharge coefficient curve fit is only valid when the venturi nozzle throat Reynolds number (Re_{dth}) is between 10^5 and 10^7, and its 95% uncertainty band is ±0.5%.

The real gas critical flow coefficient, C_R, can be estimated using the following relationship, described in MFC-7M-1987:

$$C_R = P^* V^* / (\sqrt{R T_t} P_t) \quad (3\text{-}5)$$

Several complications are likely to arise when calculating air flow using the previously described approach in a combustor heated free-jet blow down facility. Among these are:

1. Inlet conditions between engine-on (hot) runs and airflow measurement, engine-off (cold) runs must be matched as closely as possible in order to get accurate assessments of airflow during hot runs.
2. Vitiated inlet airflow makes calculating gas constant and ratio of specific heats of the test flow more complicated, since it depends on the fuel/oxidant ratio of the combustion process.

The first obstacle is addressed by relating the test conditions from the cold flow run to the hot flow run. To do this the inlet capture stream tube cross-sectional area must be calculated based on the cold flow data. This cross-sectional area can be calculated using the rearranged continuity equation:

$$A_0 = \frac{\dot{m}}{\rho V} = \frac{\dot{m}}{P_{t0c} M_{0c}} \sqrt{\frac{R T_{t0c}}{\gamma}} \left(1 + \frac{\gamma - 1}{2} {M_{0c}}^2\right)^{\frac{1+\gamma}{2(\gamma-1)}} \quad (3\text{-}6)$$

A_0 is assumed not to have changed between the cold and hot flow runs if the engine inlet conditions (inlet total pressure, total temperature, freestream Mach number, etc.) of the two runs are reasonably close. Thermal expansion in the inlet will be essentially the same between the hot and cold runs for identical inlet conditions. Engine airflow rate can then be calculated for the hot flow run by rearranging Eq. (3-6) to solve for $\dot{m}$.

$$\dot{m} = \frac{A_0 P_{t0} M_0}{\sqrt{\frac{R T_{t0}}{\gamma}} \left(1 + \frac{\gamma - 1}{2} {M_0}^2\right)^{\frac{1+\gamma}{2(\gamma-1)}}} \quad (3\text{-}7)$$

The second obstacle can be mitigated through the use of sophisticated gas properties programs that combine experimental data and chemistry equations to arrive at bulk property values for gas mixtures.

Engine Net Thrust

In free-jet engine testing, obtaining the engine net thrust is more than simply reading or recording a scale force from a thrust stand. The scale force reading from the thrust stand includes ram force from the air impacting the test article and thrust stand and pressure forces acting on the thrust stand. Net thrust is difficult to calculate in a free-jet test because of the complex interactions between the test article and the test facility. The main difficulty arises in determining the drag force on the test article. A free body diagram of is shown in Figure 10.

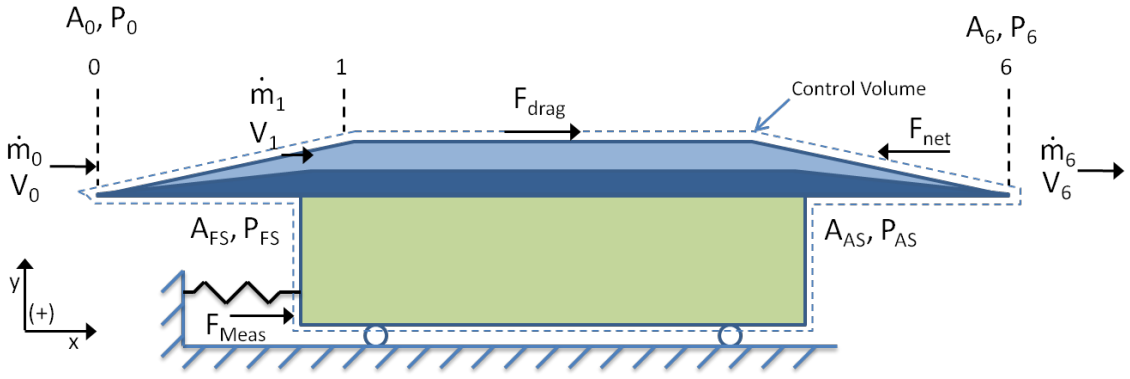

Figure 10: Free body diagram of a ramjet engine in a free-jet test

For free-jet testing the calculation of net thrust is done in two steps. Data are first acquired with air flowing on condition but without the engine running. This is called a cold flow run. These data are used to calculate the net thrust of the test article using stream thrust calculations at the engine inlet and nozzle, with assumed nozzle stream thrust efficiency, which would typically be acquired through component testing. The equation used to calculate cold flow net thrust using stream thrust functions is:

$$F_{net_C} = \eta_{Noz} * Sa_{6I} - Sa_0 - P_0 * (A_6 - A_0) \quad (3\text{-}8)$$

Where:

$$Sa_0 = \dot{m} * V_0 + P_0 * A_0$$

$$Sa_{6I} = \dot{m} * V_{6I} + P_6 * A_{6Eff}$$

$$V_{6I}, A_{6Eff} = f(P_{t5}, T_{t5}, P_6, \dot{m})$$

Sa_{6I} is the ideal nozzle stream thrust based on assuming that the flow is isentropically expanded to the ambient pressure.

With F_{net_C} the drag force can be determined as:

$$F_{drag} = F_{net_C} - F_{meas_C} - P_{FS_C} * A_{FS} + P_{AS_C} * A_{AS} \quad (3\text{-}9)$$

F_{drag} consists of drag due to friction, external aerodynamics, and ram force from the free-jet air impinging on the engine and thrust stand and is assumed to be the same for cold and hot runs. It does not take into account pressure forces on the thrust stand because these are likely to change between engine-off and engine-on runs.

Next, data are acquired at the same conditions with the engine running (hot run). Measurements from the hot flow run and F_{drag} are fed into the following equation:

$$F_{net} = F_{meas} + F_{drag} - P_{AS} * A_{AS} + P_{FS} * A_{FS} \quad (3\text{-}10)$$

The net thrust equation accounts for pressure differences on the test stand and on the engine exhaust nozzle during both the cold and hot runs. It is important to take into account the pressure forces because the nozzle exit will likely be at a different pressure

due to the combustion upstream. In addition, running the engine can alter the pumping characteristics of the exhaust facility and cause differences in cell pressure, and as a result, differences in the pressure forces exerted on the engine test stand must be included in the thrust evaluation.

Specific Impulse

Specific impulse, I_{SP}, is a measure of engine propulsive efficiency. It is defined as the change in momentum per amount of on-board propellant used and has units of seconds. A higher I_{SP} means that less fuel is required for a given change in momentum, which is a sign of higher efficiency. I_{SP} is typically used to describe the performance of rockets and air-breathing jet engines, including turbine engines, ramjets, and scramjets. Traditional chemical rockets, both solid and liquid, typically have a lower I_{SP} relative to air-breathing engines due to the fact that rockets must carry their own oxidizer, which is a component of the on-board propellant. Air-breathing engines gather their oxidizer from the atmosphere, rather than having to carry it with them, which significantly decreases the amount of propellant required and increases I_{SP}.

The equation for air-breathing I_{SP} is given in Eq. (3-11). It is simply the net thrust from the engine divided by the mass flow rate of fuel required and multiplied by the gravitational acceleration at sea level.

$$I_{SP} = \frac{F_{net}}{\dot{m}_{fuel} * g_0} \tag{3-11}$$

During an engine test, fuel mass flow is typically calculated from measurements made by calibrated turbine flowmeters. SAE ARP 4990 (Turbine Flowmeter Fuel Flow Calculations, 1997) describes the proper method to calculate fuel mass flow rate using turbine flowmeters. A turbine flowmeter, a diagram of which is shown in Figure 11, is a volumetric flow measurement device that uses the fluid flow to spin a small turbine. The device is installed in the fuel line, and an electronic pickup measures each time a turbine blade passes to determine the frequency at which the turbine is spinning. Higher flow

rates cause the turbine to spin faster. Mass flow rate is then determined as volumetric flow rate multiplied by the fluid density.

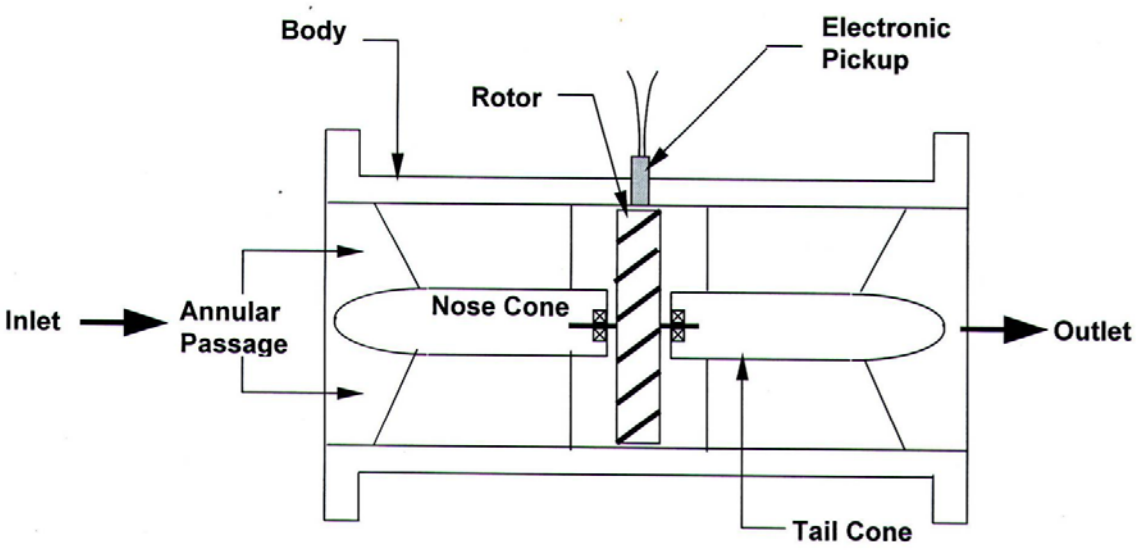

Figure 11: Turbine flowmeter diagram

SAE ARP 4990 specifies that a flowmeter must be calibrated prior to use. If the measured fluid cannot be used itself in the calibration, it should be conducted with a surrogate fluid that matches the density and viscosity of the fluid to be measured. The calibration should also be conducted through the entire range of expected flow rates. This range is known as the turn-down ratio, and it is described as the ratio of the highest calibrated flow rate to the lowest. The result of the calibration is a Roshko-Strouhal curve (example shown in Figure 12) that relates the volumetric flow rate through the meter to the frequency measured by the electronic pickup and takes into account variations in pressure, temperature, and viscosity. The equations for Strouhal and Roshko numbers are given in Eq. (3-12) and (3-13).

$$St = \frac{fD_{fm}}{V} = \frac{\pi K {D_{fm}}^3}{4} \tag{3-12}$$

$$Ro = Re * St = \frac{f {D_{fm}}^2}{\nu} \tag{3-13}$$

Where:

$$K = \frac{f}{\dot{V}}$$

$$D_{fm} = D_{fmcal}\left[1 + \alpha\left(T_{fuel} - T_{fuelcal}\right)\right]\left[1 + \frac{D_{fmcal}(P_{fuel} - P_{fuelcal})}{2tE}\right]$$

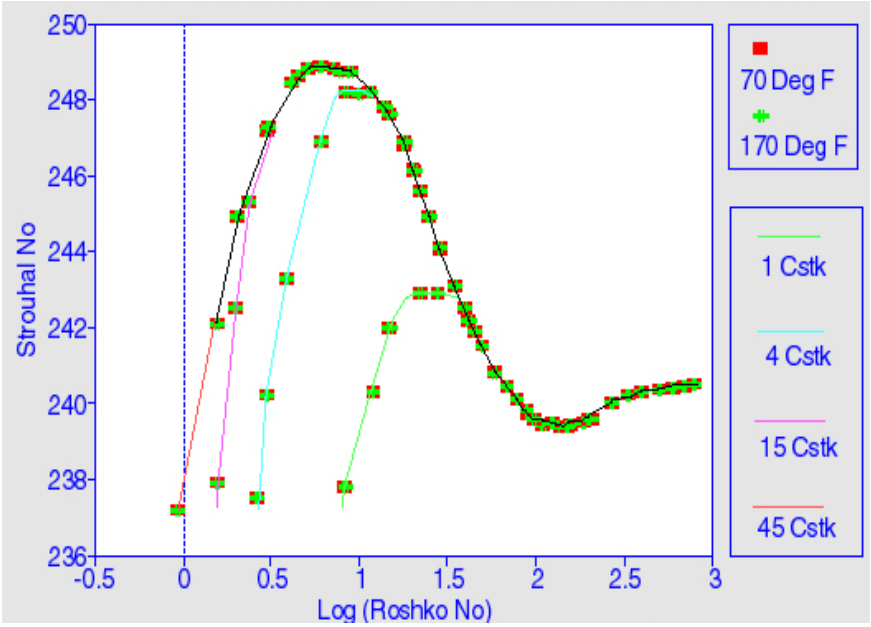

Figure 12: Fuel flow meter calibration curve at 1, 4, 15, and 45 centistokes viscosity

The steps for calculating the mass flow rate of fuel are as follows:

1. Calculate Roshko number from flowmeter frequency measurement, fuel viscosity, and flowmeter inlet pipe diameter.
2. Determine Strouhal number from the calculated Roshko number and the flowmeter calibration curve.
3. Calculate K-factor from Strouhal number and flowmeter inlet pipe diameter.
4. Calculate mass flow rate of fuel from calculated K-factor, flowmeter frequency measurement, and fuel density, see Eq. (3-14).

$$\dot{m}_{fuel} = \frac{f}{K}\rho_{fuel} \qquad (3\text{-}14)$$

Sample Data

The engine performance program was validated using a standard, accepted check case to compute the engine performance variables previously discussed and compare the program's results to the established values. The performance program data is compared to the check case data in Table 1. The table shows a sample of the outputs given by the DREPP. It shows that most differences between the check case and the DREPP are within 1%. The differences seen in TT4I, TT5, and FS6I are >1% and likely result from accumulation of errors through the DREPP calculation procedure. These calculations are dependent on other calculations, each progressive calculation adding more error. Once the model was checked out, additional calculations were made where the engine fuel flow was modulated to provide a range of engine power settings.

Table 1: DREPP Output Values Normalized by Check Case Outputs

	DREPP
A00	0.999
W00	1.000
FS00	1.003
XMFF00	1.001
XM2	0.997
TT2	1.000
PT2	1.006
FAR4	1.000
TT4I	1.014
W5	1.000
PT5	1.010
TT5	1.014
XM4	0.999
FS5	1.009
FS6I	0.983
V6	0.991
XM6	1.002
ISPF	1.000
ISPA	1.000

Figure 13 shows a graphical representation of the cross sectional areas, non-dimensionalized to physical capture area, throughout the engine. This same geometry was used with each sample set of data.

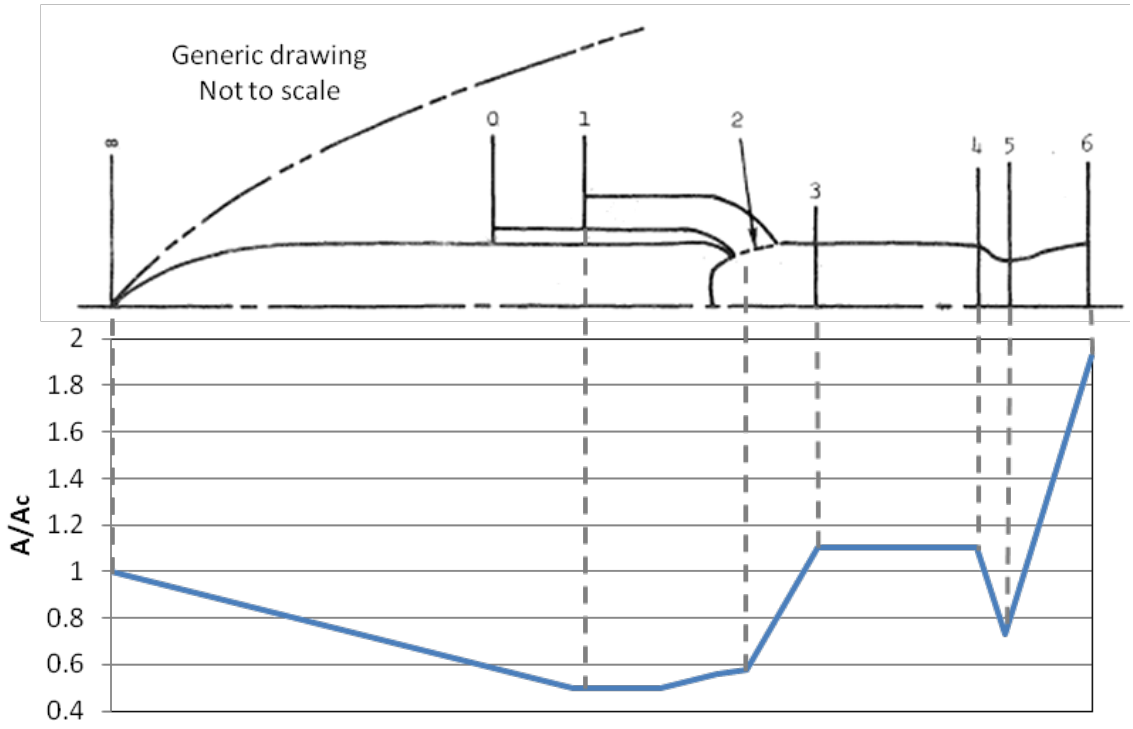

Figure 13: Non-dimensionalized cross-sectional areas through test engine

Uncertainty Analysis

Uncertainty calculations were performed using both numerical and analytical methods on the calculations for airflow, net thrust, and specific impulse. The purpose of calculating the uncertainties two ways was to define the differences in calculated uncertainty levels that might arise from using complicated numerical methods or simplified analytical methods. The numerical method is considered more accurate because it takes into account more of the complicated thermodynamic and physical interactions that occur within the engine cycle, such as the addition of fuel in the combustor. The analytical method may be employed prior to testing to get an initial

estimate of the uncertainty values. It is important to know how close the simple analytical calculations are to the more accurate numerical calculations.

Numerical Uncertainty Analysis

The numerical uncertainty analysis followed the method described in the Calculation Uncertainty section of Chapter 2 of this thesis. It employed the dithering method (Dieck, 1997) for determining sensitivity coefficients for each of the parameters that were required to calculate airflow, net thrust, and specific impulse. This method utilizes the data reduction program and changes the value of each parameter in a particular calculation individually by a small amount (in this case 0.1%), while holding all other parameter values constant, to numerically determine its effect on that calculation, forming numerical partial derivatives of the calculation with respect to each parameter. (Test Uncertainty, 2006) The sensitivity coefficients are then used in conjunction with random and systematic standard measurement uncertainties to compute an uncertainty value for a desired calculated parameter.

Simplified Analytical Uncertainty Analysis

The analytical approach used simplified equations from the data reduction program that were easily differentiable. Because the equations were easily differentiable, influence coefficients could be calculated using the methods described in the Calculation Uncertainty section of Chapter 2 of this thesis without using numerical derivatives.

The analytical equation used for airflow combines equations 3-3, 3-6, and 3-7. These equations have been combined in Eq. (3-15) with subscripts *v* and *c* added for venturi and cold flow measurement parameters, respectively. Eq. (3-15) assumes:

- $\gamma = 1.4$
- $R = 1716 \frac{ft^2}{s^2 {}^\circ R}$

$$\dot{m} = \frac{\frac{{d_{th}}^2}{4} * \pi * C_d C_R P_{tv}}{\sqrt{1716 * T_{tv}}} \frac{P_{t0}}{P_{t0c}} \sqrt{\frac{T_{t0c}}{T_{t0}}} \frac{M_0\left(1 + 0.2 * {M_{0c}}^2\right)^3}{M_{0c}\left(1 + 0.2 * {M_0}^2\right)^3} \qquad (3\text{-}15)$$

From Eq. (3-15), the analytical influence coefficients from the venturi parameters are:

- $\frac{\partial \dot{m}}{\partial d_{th}} \frac{d_{th}}{\dot{m}} = 2$
- $\frac{\partial \dot{m}}{\partial C_d} \frac{C_d}{\dot{m}} = 1$
- $\frac{\partial \dot{m}}{\partial C_R} \frac{C_R}{\dot{m}} = 1$
- $\frac{\partial \dot{m}}{\partial P_{tv}} \frac{P_{tv}}{\dot{m}} = 1$
- $\frac{\partial \dot{m}}{\partial T_{tv}} \frac{T_{tv}}{\dot{m}} = -0.5$

The analytical influence coefficients from the cold flow inlet conditions are:

- $\frac{\partial \dot{m}}{\partial P_{t0c}} \frac{P_{t0c}}{\dot{m}} = -1$
- $\frac{\partial \dot{m}}{\partial T_{t0c}} \frac{T_{t0c}}{\dot{m}} = 0.5$
- $\frac{\partial \dot{m}}{\partial M_{0c}} \frac{M_{0c}}{\dot{m}} = \frac{\left(0.6+0.04*{M_{0c}}^4+0.36*{M_{0c}}^2-\frac{1}{{M_{0c}}^2}\right)*{M_{0c}}^2}{\left(1+0.2*{M_{0c}}^2\right)^3} = \frac{5*({M_{0c}}^2-1)}{{M_{0c}}^2+5}$

The analytical influence coefficients from the hot flow inlet conditions are:

- $\frac{\partial \dot{m}}{\partial P_{t0}} \frac{P_{t0}}{\dot{m}} = 1$
- $\frac{\partial \dot{m}}{\partial T_{t0}} \frac{T_{t0}}{\dot{m}} = -0.5$
- $\frac{\partial \dot{m}}{\partial M_0} \frac{M_0}{\dot{m}} = \frac{1-{M_0}^2}{(1+0.2*{M_0}^2)^4} * (1 + 0.2 * {M_0}^2)^3 = \frac{1-{M_0}^2}{1+0.2*{M_0}^2}$

The analytical equation used to determine the influence coefficients on net thrust, Eq. (3-16), combines equations 3-8 and 3-10. Eq. (3-16) contains airflow, ideal engine nozzle exit airflow velocity, ideal engine nozzle exit effective area, and engine inlet airflow velocity ($\dot{m}$, V_{6I}, A_{6eff}, and V_0), each of which is the result of a calculation rather

than a direct measurement. For simplicity these calculations were not decomposed further to their direct measurements.

$$F_{net} = F_{meas} - F_{meas_C} + \left[\dot{m}(\eta_{noz}V_{6I} - V_0) + (\eta_{noz}P_6A_{6eff} - P_0A_6)\right]_C - A_{AS}\left(P_{AS} - P_{AS_C}\right) + A_{FS}\left(P_{FS} - P_{FS_C}\right) \quad (3\text{-}16)$$

Using this combined equation, the analytical influence coefficients for net thrust are:

- $\frac{\partial F_{net}}{\partial F_{meas}}\frac{F_{meas}}{F_{net}} = \frac{F_{meas}}{F_{net}}$
- $\frac{\partial F_{net}}{\partial F_{meas_C}}\frac{F_{meas_C}}{F_{net}} = -\frac{F_{meas_C}}{F_{net}}$
- $\frac{\partial F_{net}}{\partial \dot{m}}\frac{\dot{m}}{F_{net}} = \frac{\dot{m}\left(\eta_{noz}V_{6I_C} - V_{0_C}\right)}{F_{net}}$
- $\frac{\partial F_{net}}{\partial \eta_{noz}}\frac{\eta_{noz}}{F_{net}} = \frac{\eta_{noz}\left(P_6A_{6eff} + \dot{m}V_{6I_C}\right)}{F_{net}}$
- $\frac{\partial F_{net}}{\partial V_{6_C}}\frac{V_{6I_C}}{F_{net}} = \frac{\eta_{noz}\dot{m}V_{6I_C}}{F_{net}}$
- $\frac{\partial F_{net}}{\partial V_{0_C}}\frac{V_{0_C}}{F_{net}} = -\frac{\dot{m}V_{0_C}}{F_{net}}$
- $\frac{\partial F_{net}}{\partial P_{amb}}\frac{P_{amb}}{F_{net}} = \frac{\eta_{noz}P_{amb}A_{6eff}}{F_{net}}$
- $\frac{\partial F_{net}}{\partial A_{6eff}}\frac{A_{6eff}}{F_{net}} = \frac{\eta_{noz}P_{amb}A_{6eff}}{F_{net}}$
- $\frac{\partial F_{net}}{\partial P_0}\frac{P_0}{F_{net}} = -\frac{P_0A_6}{F_{net}}$
- $\frac{\partial F_{net}}{\partial A_6}\frac{A_6}{F_{net}} = -\frac{P_0A_6}{F_{net}}$
- $\frac{\partial F_{net}}{\partial A_{AS}}\frac{A_{AS}}{F_{net}} = \frac{A_{AS}\left(P_{AS_C} - P_{AS}\right)}{F_{net}}$
- $\frac{\partial F_{net}}{\partial P_{AS}}\frac{P_{AS}}{F_{net}} = -\frac{A_{AS}P_{AS}}{F_{net}}$
- $\frac{\partial F_{net}}{\partial P_{AS_C}}\frac{P_{AS_C}}{F_{net}} = \frac{A_{AS}P_{AS_C}}{F_{net}}$

- $\frac{\partial F_{net}}{\partial A_{FS}} \frac{A_{FS}}{F_{net}} = \frac{A_{FS}\left(P_{FS} - P_{FS_C}\right)}{F_{net}}$
- $\frac{\partial F_{net}}{\partial P_{FS}} \frac{P_{FS}}{F_{net}} = \frac{A_{FS} P_{FS}}{F_{net}}$
- $\frac{\partial F_{net}}{\partial P_{FS_C}} \frac{P_{FS_C}}{F_{net}} = -\frac{A_{FS} P_{FS_C}}{F_{net}}$

Fuel specific impulse, as described in Eq. (3-11), is simply the net thrust divided by fuel flow multiplied by the gravitational constant. The influence coefficient of net thrust on specific impulse is one, which means that all of the influence coefficients from net thrust apply directly to the specific impulse calculation. The only remaining influence coefficients to calculate are those for the mass flow calculation. Equation (3-17) is the result of combining the fuel flow equation, Eq. (3-14), with Eq. (3-11).

$$I_{SP} = \frac{F_{net}}{\frac{f}{K} \rho_{fuel} * g_0} \tag{3-17}$$

The analytical influence coefficients for the fuel flow part of the specific impulse equation are:

- $\frac{\partial I_{SP}}{\partial f} \frac{f}{I_{SP}} = -1$
- $\frac{\partial I_{SP}}{\partial K} \frac{K}{I_{SP}} = 1$
- $\frac{\partial I_{SP}}{\partial \rho_{fuel}} \frac{\rho_{fuel}}{I_{SP}} = -1$

CHAPTER IV

RESULTS AND DISCUSSION

A data reduction computer program was developed for this thesis and was written in Matlab®. A check case was used in the data reduction program, and the results of the check case compared favorably to known results. One of the major difficulties with the model was its input requirements. The techniques outlined in the approach were designed to be used with experimental data, where parameters like scale force and flow meter frequency are measured values. Working backwards from the final answer to the measured value was required when using data from textbooks.

Performance Analysis

One ramjet flight condition was analyzed at multiple power settings for this thesis. The flight condition was 80,000 feet at a Mach number of 4.1. The power setting was modulated by adjusting the fuel flow supplied to the engine.

Figure 14 shows I_{SP} versus combustor fuel-to-air mass ratio (FAR4) for the range of fuel flows analyzed. The shape of the curve is typical of engine tests where power is modulated from low to high. The data show that, at FAR4 of 0.05, the engine reaches a maximum I_{SP}. This is the most efficient power setting for the engine at this particular flight condition.

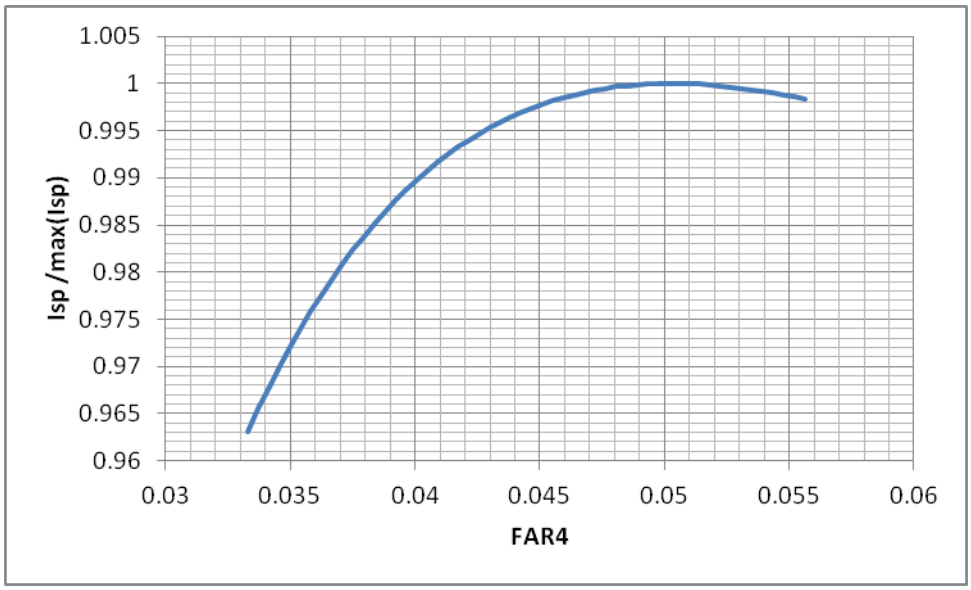

Figure 14: Non-dimensionalized specific impulse versus fuel-to-air mass ratio at 80k, Mach 4.1

Figure 15 shows the change in specific net thrust (net thrust per pound-mass of airflow) with respect to FAR4. As FAR4 (fuel flow) increases, specific net thrust increases proportionally, as expected.

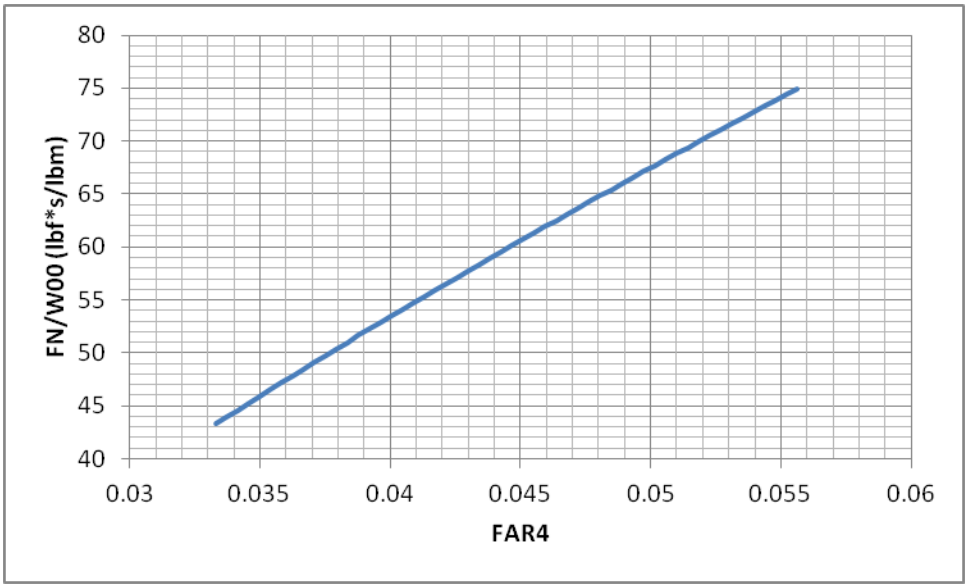

Figure 15: Net thrust per airflow versus fuel-to-air mass ratio at 80k, Mach 4.1

Uncertainty Analysis

The goal of the uncertainty analysis was to determine which input parameters had the greatest contribution to the uncertainty of the airflow, net thrust, and specific impulse calculations. This was accomplished by using the performance computer program based on the methods laid out in Chapter III, perturbing each of the input parameters by a small amount, and calculating the change in airflow, specific impulse, and net thrust. The relative change in calculated parameter divided by the relative change in perturbed parameter yields the influence coefficient. A small perturbation value was required to numerically approximate the partial derivative of the calculation with respect to the input parameter. A parametric study was conducted to determine how much the influence coefficient changed with perturbations of ±0.1%, ±0.5%, and ±1%. The results of this parametric study are tabulated in Appendix A, and the influence coefficients that follow are calculated from the average of the +0.1% and -0.1% perturbations.

Influence coefficients are used to determine which parameters are the biggest drivers in the uncertainty of a calculation. For example, an influence coefficient of 2 for parameter x on calculation y implies that for a 1% change in x, y changes by 2%. With this information, experimenters can more effectively minimize the overall uncertainty of calculations by choosing to improve the elemental measurements that have the largest impact on the calculation over those that have little or no impact.

Only influence coefficients of 0.001 or greater are displayed below. All others were deemed too insignificant and ignored. The numerical influence coefficients are also compared to their corresponding analytical counterpart, where applicable.

Airflow

The analytical influence coefficients for airflow were calculated using Eq. (3-15). It contains freestream Mach number, which is not a direct measurement; it is calculated in a test cell environment the nozzle inlet flow total pressure, total temperature, and the nozzle exit or test cell static pressure. The performance program was utilized to find numerical influence coefficients for airflow using a given freestream Mach number for comparison with the analytical values, and also modified and run using total pressure,

total temperature, and static pressure to calculate the freestream Mach number. The latter method better represents a real world example in a ground test environment.

The influence coefficients for the airflow calculation in which freestream Mach number is an input are tabulated in Table 2 and shown graphically in Figure 16.

Table 2: Non-dimensional influence coefficients for airflow rate uncertainty calculation with freestream Mach number input

Parameter	IC (%/100)		Description
	Numerical	Analytical	
P_{t0c}	-1.0000	-1	Freestream total pressure, cold flow
T_{t0c}	0.5000	0.5	Freestream total temperature, cold flow
M_{0c}	4.0956	3.624	Freestream Mach number, cold flow
P_{tv}	1.0000	1	Airflow Venturi total pressure
T_{tv}	-0.5000	-0.5	Airflow Venturi total temperature
d_{th}	2.0000	2	Airflow Venturi throat area
C_d	1.0000	1	Airflow Venturi discharge coefficient
C_r	1.0000	1	Airflow Venturi real gas critical flow coefficient
T_{t0}	-0.3445	-0.5	Freestream total temperature, hot flow
P_{t0}	0.9998	1	Freestream total pressure, hot flow
M_0	-3.6130	-3.624	Freestream Mach number, hot flow

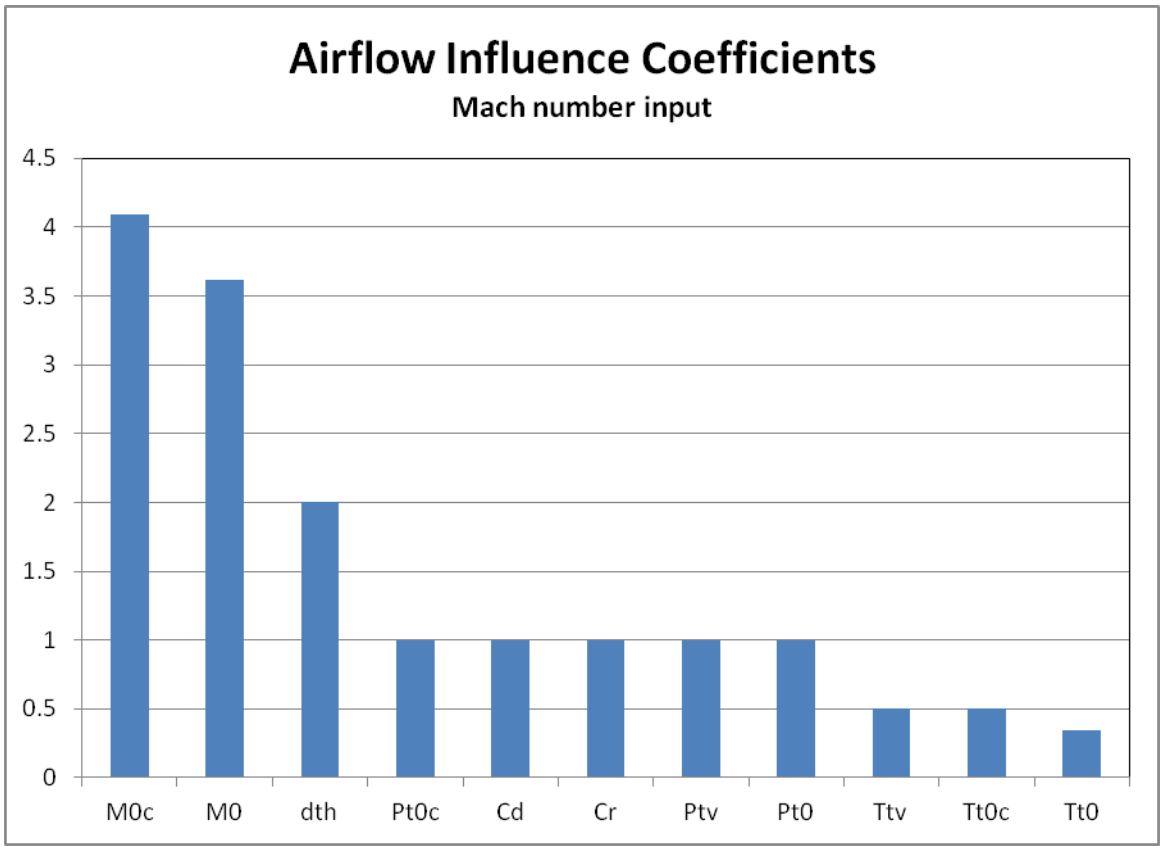

Figure 16: Chart of non-dimensional numerical influence coefficients for airflow rate uncertainty with freestream Mach number input

Airflow uncertainty was found to be heavily influenced by the freestream Mach number, both during a run with an airflow measurement device in place in the engine flow path (engine-off or cold run) and the engine-on performance run (hot run), with absolute values of 4.10 and 3.61, respectively. The analytical equations for engine-off and engine-on freestream Mach number show that these values are asymptotically approaching 5.

With the exception of cold flow freestream Mach number, M_{0c}, and hot flow freestream total temperature, T_{t0}, all of the numerically and analytically calculated influence coefficients matched within about 0.01. The precise reason for the difference seen in M_{0c} and T_{t0} is currently unknown, but what this difference implies is that both parameters have an additional influence on the airflow calculation that is not being captured in the analytical method.

The simplified analytical approach could be used to quickly calculate an uncertainty value for airflow, if needed. The elemental uncertainty value used for Mach number would likely need to be a Type-B uncertainty that is based on "engineering judgment" of the test facility and its ability to produce a desired Mach number.

The influence coefficients for airflow rate using inlet total pressure, total temperature, and static pressure to calculate inlet Mach number are tabulated in Table 3 and shown graphically in Figure 16.

Table 3: Non-dimensional influence coefficients for airflow rate uncertainty calculation with calculated freestream Mach number

Parameter	IC (%/100)	Description
	Numerical	
P_{t0c}	-0.2372	Freestream total pressure, cold flow
T_{t0c}	0.3812	Freestream total temperature, cold flow
P_{0c}	-0.7607	Freestream static pressure, cold flow
P_{tv}	1.0000	Airflow Venturi total pressure
T_{tv}	-0.4996	Airflow Venturi total temperature
d_{th}	2.0010	Airflow Venturi throat area
C_d	1.0000	Airflow Venturi discharge coefficient
C_r	1.0000	Airflow Venturi real gas critical flow coefficient
T_{t0}	-0.2400	Freestream total temperature, hot flow
P_{t0}	0.3269	Freestream total pressure, hot flow
P_0	0.6715	Freestream static pressure, hot flow

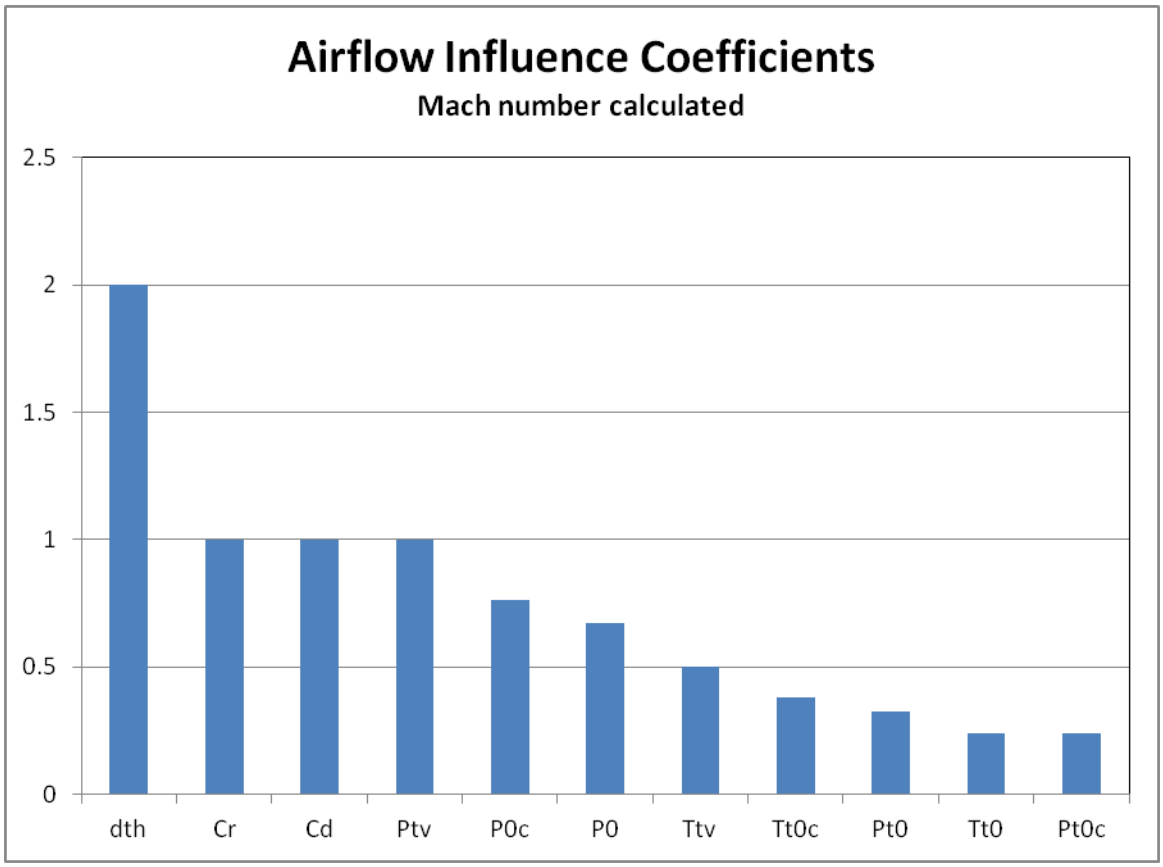

Figure 17: Chart of non-dimensional numerical influence coefficients for airflow rate uncertainty with freestream Mach number calculated

The differences between the two sets of influences coefficients displayed in Table 2 and Table 3 are apparent in the freestream conditions. The freestream total pressure influence coefficient with freestream Mach number as an input is split into a static and total pressure influence coefficient when freestream Mach number is calculated. The freestream total temperature influence coefficient was also reduced slightly. With the large freestream Mach number influence coefficients gone, the major uncertainty driver is the airflow measurement venturi throat diameter, d_{th}.

Net Thrust

The influence coefficients for net thrust are tabulated in Table 4 and shown graphically in Figure 18. Figure 18 also distinguishes between influence coefficients that

affect the net thrust calculation only through the airflow calculation, influence coefficients that only affect the net thrust calculation, and influence coefficients that affect the net thrust calculation directly and through the airflow calculation.

Table 4 shows that, with most parameters, the analytical method predicts the net thrust influence coefficients very well. Differences are only seen in hot flow freestream static pressure (P_0), ambient cell pressure (P_{amb}), and nozzle stream thrust efficiency (η_n).

Table 4 contains analytical influence coefficient values for cold flow ideal nozzle exit velocity, cold flow freestream velocity, cold flow airflow, and effective nozzle exit area under ideal expansion to ambient pressure. Each of these parameters is actually a calculation that was not further decomposed to its elemental measurements. This was done to simplify the analytical equation for net thrust. In the case of cold flow airflow and freestream velocity, it was done to reduce the number of parameters in the equation. Cold flow ideal nozzle exit velocity and effective nozzle exit area under ideal expansion to ambient pressure, however, were not decomposed because they are calculated in the DREPP using an iterative process that cannot be replicated analytically.

The hot flow freestream static pressure and ambient cell pressure are used in the DREPP to calculate engine airflow and ideal nozzle exit velocity, respectively, as well as net thrust. Since the analytical method did not break down the calculation for airflow or ideal nozzle exit velocity into their components for simplicity, the values for P_0 and P_{amb} only represent their effects directly on net thrust; their effects on airflow ideal nozzle exit velocity are captured within the their respective influence coefficient for net thrust.

The largest difference lies in the nozzle stream thrust efficiency. The reason for this difference is likely a result of the analytical nozzle stream thrust efficiency equation being a function of effective nozzle exit area and ideal nozzle exit velocity. These parameters were iteratively calculated in the DREPP and essentially treated as measurements in the analytical solution for simplicity.

The analytical equations for the measured scale force influence coefficients (engine-off and engine-on) are the measured scale force divided by the calculated net force. This means that these influence coefficients approach zero as measured scale force approaches zero. During engine-on tests, it is not uncommon for scale force to read close

to zero because the drag forces on the engine and test stand are typically of the same order as thrust produced by the engine.

Table 4: Non-dimensional influence coefficients for uncertainty in net thrust calculation

Parameter	IC (%/100)		Description
	Numerical	Analytical	
P_{t0c}	0.0038		Free stream total pressure, cold flow
T_{t0c}	-0.0062		Free stream total temperature, cold flow
P_{0c}	0.0123		Free stream static pressure, cold flow
P_{tv}	-0.0164		Airflow Venturi total pressure
T_{tv}	0.0081		Airflow Venturi total temperature
d_{th}	-0.0330		Airflow Venturi throat area
C_d	-0.0164		Airflow Venturi discharge coefficient
C_r	-0.0164		Airflow Venturi real gas critical flow coefficient
T_{t0}	-0.0152		Free stream total pressure, hot flow
P_{t0}	-0.1375		Free stream total temperature, hot flow
P_0	-0.0450	-0.270209	Free stream static pressure, hot flow
A_5	-0.1590		Nozzle throat area
C_{dn}	0.1592		Nozzle discharge coefficient
P_{amb}	-0.2638	-0.2702	Ambient pressure
A_6	-0.2702	-0.2702	Nozzle exit area
F_{meas}	-1.7121	-1.7121	Measured scale force, hot flow
P_{AS}	-0.0796	-0.0796	Nozzle exit base pressure, hot flow
P_{FS}	0.1115	0.1115	Pylon base pressure, hot flow
F_{measc}	3.1303	3.1303	Measured scale force, cold flow
P_{ASc}	0.0908	0.0908	Nozzle exit base pressure, cold flow
A_{AS}	0.0111	0.0111	Nozzle exit base area
P_{FSc}	-0.0955	-0.0955	Pylon base pressure, cold flow
A_{FS}	0.0159	0.0159	Pylon base area
η_n	2.4764	3.8807	Nozzle stream thrust efficiency
F_{netc}	-0.4453	-0.4453	Net thrust, cold flow
V_{6Ic}		3.5128	Station 6 velocity, cold flow
V_{0c}		-2.7024	Free stream velocity, cold flow
m_{dot}		0.8104	Airflow
A_{6eff}		0.3679	Effective nozzle exit area, ideal expansion

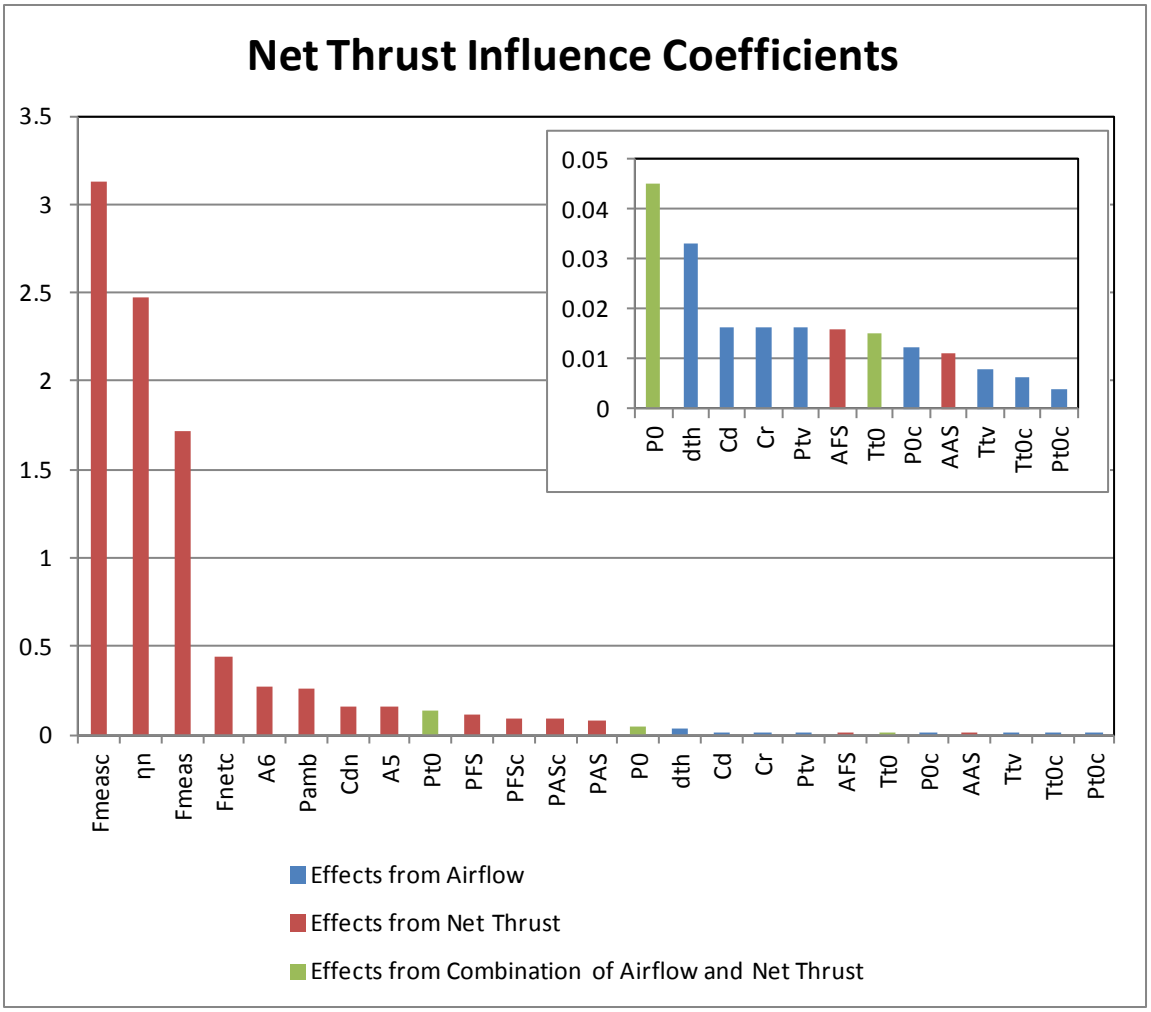

Figure 18: Chart of non-dimensional numerical influence coefficients for net thrust uncertainty calculation

Specific Impulse

The influence coefficients for specific impulse are tabulated in Table 5 and shown graphically in Figure 19. As with Figure 18, Figure 19 also makes a distinction between influence coefficients that come from airflow and net thrust calculations and those that are unique to the specific impulse calculation.

Table 5: Non-dimensional influence coefficients for uncertainty in specific impulse uncertainty calculation

Parameter	IC (%/100)		Description
	Numerical	Analytical	
P_{t0c}	0.0038		Free stream total pressure, cold flow
T_{t0c}	-0.0062		Free stream total temperature, cold flow
P_{0c}	0.0123		Free stream static pressure, cold flow
P_{tv}	-0.0162		Airflow Venturi total pressure
T_{tv}	0.0081		Airflow Venturi total temperature
d_{th}	-0.0324		Airflow Venturi throat area
C_d	-0.0162		Airflow Venturi discharge coefficient
C_r	-0.0162		Airflow Venturi real gas critical flow coefficient
T_{t0}	-0.0152		Free stream total pressure, hot flow
P_{t0}	-0.1373		Free stream total temperature, hot flow
P_0	-0.0448	-0.270209	Free stream static pressure, hot flow
K	1.0000	1	Fuel flowmeter calibration table
T_{op}	0.2528		Fuel temperature at flowmeter
T_{cal}	0.0150		Fuel temperature during flowmeter calibration
SG_{60f}	-1.0036	-1	Specific gravity of fuel at 60°F
f	-0.9998	-1	Fuel flowmeter frequency
A_5	-0.1589		Nozzle throat area
C_{dn}	0.1589		Nozzle discharge coefficient
P_{amb}	-0.2638	-0.2702	Ambient pressure
A_6	-0.2702	-0.2702	Nozzle exit area
F_{meas}	-1.7121	-1.7121	Measured scale force, hot flow
P_{AS}	-0.0796	-0.0796	Nozzle exit base pressure, hot flow
P_{FS}	0.1115	0.1115	Pylon base pressure, hot flow
F_{measc}	3.1303	3.1303	Measured scale force, cold flow
P_{ASc}	0.0908	0.0908	Nozzle exit base pressure, cold flow
A_{AS}	0.0111	0.0111	Nozzle exit base area
P_{FSc}	-0.0955	-0.0955	Pylon base pressure, cold flow
A_{FS}	0.0159	0.0159	Pylon base area
η_n	2.4764	3.8807	Nozzle stream thrust efficiency
F_{netc}	-0.4453	-0.4453	Net thrust, cold flow
V_{6Ic}		3.5128	Station 6 velocity, cold flow
V_{0c}		-2.7024	Free stream velocity, cold flow
m_{dot}		0.8104	Airflow
A_{6eff}		0.3679	Effective nozzle exit area, ideal expansion

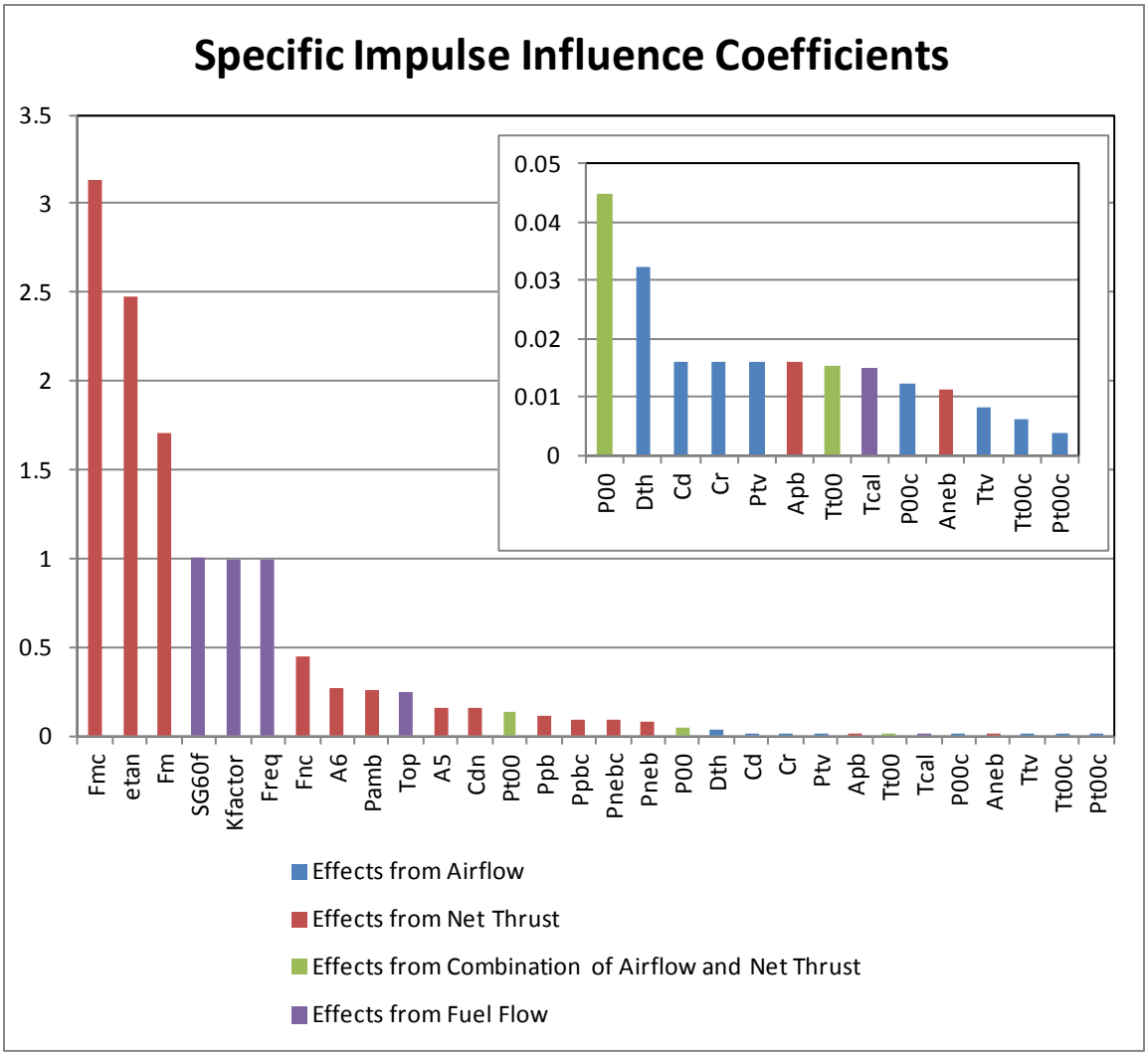

Figure 19: Chart of non-dimensional numerical influence coefficients for fuel specific impulse uncertainty calculation

Specific impulse is a ratio of net thrust to fuel flow, with each contributing equally to the overall uncertainty. The influence coefficient of net thrust on specific impulse is 1. For this reason, each of the influence coefficients for net thrust equally affects specific impulse.

The numerical influence coefficients from fuel flow parameters matched very well, within about 0.004, with their analytical analogues. The numerical calculation showed that two parameters that were not included in the analytical analysis, T_{op} and T_{cal},

had a small but calculable influence on specific impulse. T_{op} is the temperature of the fuel being measured. It is used to make corrections to the specific gravity and viscosity of the fluid, and it is also used in conjunction with T_{cal} to make thermal corrections to the flowmeter calibration.

CHAPTER V

CONCLUSIONS AND RECOMMENDATIONS

The work performed in this thesis has helped to further the understanding of the major uncertainty drivers for airflow, net thrust, and specific impulse during a ramjet engine test in a free-jet test cell.

In the airflow calculation the analysis of uncertainty contributors showed that, in order to gain the greatest decrease in overall airflow uncertainty, increasing measurement accuracy in the mass flow measuring venturi nozzle total pressure, hot flow and cold flow freestream static pressures, and venturi nozzle total temperature would show the greatest overall uncertainty benefit, greater than in the freestream total pressures and temperatures. This assumes that the venturi nozzle throat diameter uncertainty is already low enough to be negligible and that the venturi nozzle calculations are performed according to MFC-7M-1987, which defines an uncertainty value for C_R and C_d. If necessary C_R and C_d could be reduced further by calibration of the venturi nozzle.

The uncertainty of the net thrust equation is dominated by the uncertainty in the scale force measurement in both hot and cold flow (F_{meas}, $F_{meas,c}$) as well as the nozzle stream thrust efficiency (η_{noz}). Some ways to reduce the scale force uncertainty include:

- Using a more accurate measurement device.
- Designing the experiment such that, when running, scale force is close to zero.
- Performing better calibrations on the measurement device, including calibrations to account for pressure effects if using a sealed load cell.
- Calibrating the engine test stand to determine the effects due to resistance to motion (tare) and hysteresis.
- Making sure that the tare due to fuel lines and instrumentation lines entering the pedestal is properly accounted for.

Uncertainty on nozzle stream thrust efficiency will need to be addressed in component testing of the nozzle. Any methods used during component testing to decrease the overall

uncertainty of this parameter will have a large effect on the overall net thrust uncertainty when using the method outlined in this thesis.

Since I_{SP} contains all of the uncertainty contributors of the net thrust calculation, all efforts made to decrease net thrust uncertainty will also decrease I_{SP} uncertainty. In addition I_{SP} uncertainty is also influenced by fuel flow calculation parameters. The specific gravity of the fuel being used, the flowmeter calibration, and the frequency measurement from the flowmeter all equally affect the overall I_{SP} uncertainty. The specific gravity uncertainty can be minimized by acquiring fuel samples prior to and after a test and having them analyzed by a chemical lab using an accepted industry standard, such as ASTM D4052. The flowmeter calibration uncertainty can be reduced by using a more accurate calibration rig and calibrating the flowmeter multiple times over the flow range that it is expected to see during testing. The uncertainty of the flowmeter frequency measurement can be minimized by ensuring that the proper flowmeter is used for the expected flow rates.

This computer performance model was validated in this thesis using an accepted check case because engine test experimental data is not readily available to the public. Additional validation will be done in the future using experimental data to increase the credibility of the model. Currently the model works for ramjet cases, where the flow through the engine combustor becomes completely subsonic. Future work will be done to modify the performance program to allow dual-mode ramjet and scramjet analysis.

WORKS CITED

Coleman, H., & Steele, G. (1999). *Experimentation and Uncertainty Analysis for Engineers* (2nd ed.). New York, NY: John Wiley & Sons.

Dessornes, O., Scherrer, D., & Novelli, R. (2001). *Tests of the JAPHAR Dual Mode Ramjet Engine.* Office National d'Etudes et de Recherches Aerospatiale. Chatillon, France: American Institute of Aeronautics and Astronautics.

Dieck, R. (1997). *Measurement Uncertainty: Methods and Applications* (2nd ed.). Research Triangle Park, NC: Instrument Society of America.

Dunsworth, L., & Reed, G. *Ramjet Engine Testing Simulation Techniques.* American Institute of Aeronautics and Astronautics.

Duveau, P., Hallard, R., Novelli, P., & Eggers, T. (1999). *Aerodynamic Performance Analysis of the Hypersonic Airbreathing Vehicle JAPHAR.* International Society for Air Breathing Engines.

(2008). *Evaluation of measurement data - Guide to the expression of uncertainty in measurement.* Joint Committee for Guides in Metrology.

Falempin, F. (2008). Ramjet and Dual Mode Operation. *Advances on Propulsion Technology for High-Speed Aircraft* .

Fetterhoff, T., Bancroft, S., Burfitt, W., Osborne, J., Hawkins, W., & Schulz, R. J. (2011). *Advanced Propulsion Test Technology Hypersonic Test Methodology Study: Test Media Effects on Scramjet Engines in Shock and Blowdown Facilities.* ISABE.

Goyne, C., Crisci, D., & Fetterhoff, T. (2009). Short Duration Propulsion Test and Evaluation (Hy-V) Program. *16th AIAA/DLR/DGLR International Space Planes and Hypersonic Systems and Technologies.* American Institute of Aeronautics and Astronautics.

(1994). *Guidelines for Evaluating and Expressing the Uncertainty of NIST Measurement Results.* National Institute of Standards and Technology.

Heiser, W., & Pratt, D. (1994). *Hypersonic Airbreathing Propulsion.* Washington, DC: American Institute of Aeronautics and Astronautics, Inc.

(2008). *International vocabulary of metrology - Basic and general concepts and associated terms.* Joint Committee for Guides in Metrology.

McVey, J. (1976). *Recommended Ramburner Test Reporting Standards.* Johns Hopkins University, Applied Physics Lab. Laurel, MD: Chemical Propulsion Information Agency.

(1987). *Measurement of Gas Flow by Means of Critical Flow Venturi Nozzles.* New York, NY: American Society of Mechanical Engineers.

Smart, M., & Ruf, E. (2006). *Free-jet Testing of a REST Scramjet at Off-Design Conditions.* NASA Langley Research Center. Hampton, VA: American Institute of Aeronautics and Astronautics.

Smith, S., Scheid, A., Eklund, D., Gruber, M., Wilkin, H., & Mathur, T. (2008). *Supersonic Combustion Research Laboratory Uncertainty Analysis.* Hartford, CT: 44th AIAA/ASME/SAE/ASEE Joint Propulsion Conference and Exhibit.

Smith, V. K. *Ground Testing Aeropropulsion Systems: An Overview.* Aerospace Testing Alliance.

(2006). *Test Uncertainty.* American Society of Mechanical Engineers.

(1997). *Turbine Flowmeter Fuel Flow Calculations.* Warrendale, PA: Society of Automotive Engineers.

Voland, R., Auslender, A., Smart, M., Roudakov, A., Semenov, V., & Kopchenov, V. (1999). *CIAM/NASA Mach 6.5 Scramjet Flight and Ground Test.* American Institute of Aeronautics and Astronautics.

APPENDIX

Table A1: Parametric study of airflow influence coefficients with inlet Mach number input

Parameter	IC						Spread	Description
	-0.01	-0.005	-0.001	+0.001	+0.005	+0.01		
Pt00c	-1.0101	-1.0050	-1.0010	-0.9990	-0.9950	-0.9901	0.0032	Free stream total pressure, cold flow
Tt00c	0.5013	0.5006	0.5001	0.4999	0.4994	0.4988	0.0047	Free stream total temperature, cold flow
M00c	4.0198	4.0575	4.0879	4.1033	4.1341	4.1730	0.0137	Free stream Mach number, cold flow
Ptv	1.0000	1.0000	1.0000	1.0000	1.0000	1.0000	0.0000	Airflow Venturi total pressure
Ttv	-0.5038	-0.5019	-0.5004	-0.4996	-0.4981	-0.4963	0.0075	Airflow Venturi total temperature
Dth	1.9900	1.9950	1.9990	2.0010	2.0050	2.0100	0.0200	Airflow Venturi throat area
Cd	1.0000	1.0000	1.0000	1.0000	1.0000	1.0000	0.0000	Airflow Venturi discharge coefficient
Cr	1.0000	1.0000	1.0000	1.0000	1.0000	1.0000	0.0000	Airflow Venturi real gas critical flow coefficient
Tt00	-0.3496	-0.3570	-0.3443	-0.3446	-0.3452	-0.3459	0.0023	Free stream total pressure, hot flow
Pt00	0.9998	0.9998	0.9998	0.9998	0.9998	0.9998	0.0024	Free stream total temperature, hot flow
M00	-3.6937	-3.6632	-3.6203	-3.6057	-3.5768	-3.5410	0.0024	Free stream Mach number, hot flow

Table A2: Parametric study of airflow influence coefficients with calculated inlet Mach number

Parameter	IC						Spread	Description
	-0.01	-0.005	-0.001	+0.001	+0.005	+0.01		
Pt00c	-0.2390	-0.2382	-0.2375	-0.2372	-0.2357	-0.2357	0.0032	Free stream total pressure, cold flow
Tt00c	0.3838	0.3826	0.3817	0.3812	0.3791	0.3791	0.0047	Free stream total temperature, cold flow
P00c	-0.7683	-0.7648	-0.7621	-0.7607	-0.7546	-0.7546	0.0137	Free stream static pressure, cold flow
Ptv	1.0000	1.0000	1.0000	1.0000	1.0000	1.0000	0.0000	Airflow Venturi total pressure
Ttv	-0.5038	-0.5019	-0.5004	-0.4996	-0.4963	-0.4963	0.0075	Airflow Venturi total temperature
Dth	1.9900	1.9950	1.9990	2.0010	2.0100	2.0100	0.0200	Airflow Venturi throat area
Cd	1.0000	1.0000	1.0000	1.0000	1.0000	1.0000	0.0000	Airflow Venturi discharge coefficient
Cr	1.0000	1.0000	1.0000	1.0000	1.0000	1.0000	0.0000	Airflow Venturi real gas critical flow coefficient
Tt00	-0.2387	-0.2393	-0.2397	-0.2400	-0.2411	-0.2411	0.0023	Free stream total pressure, hot flow
Pt00	0.3282	0.3276	0.3272	0.3269	0.3258	0.3258	0.0024	Free stream total temperature, hot flow
P00	0.6728	0.6722	0.6718	0.6715	0.6705	0.6705	0.0024	Free stream static pressure, hot flow

Table A3: Parametric study of net thrust influence coefficients

Parameter	IC						Spread	Description
	-0.01	-0.005	-0.001	+0.001	+0.005	+0.01		
Pt00c	0.0038	0.0038	0.0038	0.0038	0.0038	0.0038	0.0000	Free stream total pressure, cold flow
Tt00c	-0.0063	-0.0062	-0.0062	-0.0062	-0.0061	-0.0061	0.0002	Free stream total temperature, cold flow
P00c	0.0121	0.0122	0.0123	0.0124	0.0125	0.0125	0.0004	Free stream static pressure, cold flow
Ptv	-0.0167	-0.0165	-0.0163	-0.0161	-0.0156	-0.0156	0.0011	Airflow Venturi total pressure
Ttv	0.0080	0.0081	0.0081	0.0081	0.0082	0.0082	0.0002	Airflow Venturi total temperature
Dth	-0.0344	-0.0334	-0.0326	-0.0322	-0.0303	-0.0303	0.0041	Airflow Venturi throat area
Cd	-0.0167	-0.0165	-0.0163	-0.0161	-0.0156	-0.0156	0.0011	Airflow Venturi discharge coefficient
Cr	-0.0167	-0.0165	-0.0163	-0.0161	-0.0156	-0.0156	0.0011	Airflow Venturi real gas critical flow coefficient
Tt00	-0.0153	-0.0152	-0.0152	-0.0152	-0.0152	-0.0152	0.0000	Free stream total pressure, hot flow
Pt00	-0.1378	-0.1376	-0.1374	-0.1373	-0.1368	-0.1368	0.0010	Free stream total temperature, hot flow
P00	-0.0455	-0.0452	-0.0449	-0.0448	-0.0441	-0.0441	0.0014	Free stream static pressure, hot flow
A5	-0.1594	-0.1591	-0.1589	-0.1588	-0.1583	-0.1583	0.0011	Nozzle throat area
Cdn	0.1599	0.1594	0.1590	0.1588	0.1578	0.1578	0.0021	Nozzle discharge coefficient
Pamb	-0.2642	-0.2639	-0.2637	-0.2636	-0.2631	-0.2631	0.0011	Ambient pressure
A6	-0.2702	-0.2702	-0.2702	-0.2702	-0.2702	-0.2702	0.0000	Nozzle exit area
Fm	-1.7121	-1.7121	-1.7121	-1.7121	-1.7121	-1.7121	0.0000	Measured scale force, hot flow
Pneb	-0.0796	-0.0796	-0.0796	-0.0796	-0.0796	-0.0796	0.0000	Nozzle exit base pressure, hot flow
Ppb	0.1115	0.1115	0.1115	0.1115	0.1115	0.1115	0.0000	Pylon base pressure, hot flow
Fmc	3.1303	3.1303	3.1303	3.1303	3.1303	3.1303	0.0000	Measured scale force, cold flow
Fnc	-0.4453	-0.4453	-0.4453	-0.4453	-0.4453	-0.4453	0.0000	Net thrust, cold flow
Pnebc	0.0908	0.0908	0.0908	0.0908	0.0908	0.0908	0.0000	Nozzle exit base pressure, cold flow
Aneb	0.0111	0.0111	0.0111	0.0111	0.0111	0.0111	0.0000	Nozzle exit base area
Ppbc	-0.0955	-0.0955	-0.0955	-0.0955	-0.0955	-0.0955	0.0000	Pylon base pressure, cold flow
Apb	0.0159	0.0159	0.0159	0.0159	0.0159	0.0159	0.0000	Pylon base area
etan	2.4764	2.4764	2.4764	2.4764	2.4764	2.4764	0.0000	Nozzle stream thrust efficiency

Table A4: Parametric study of specific impulse influence coefficients

Parameter	IC						Spread	Description
	-0.01	-0.005	-0.001	+0.001	+0.005	+0.01		
Pt00c	0.0038	0.0038	0.0038	0.0038	0.0038	0.0038	0.0000	Free stream total pressure, cold flow
Tt00c	-0.0063	-0.0062	-0.0062	-0.0062	-0.0061	-0.0061	0.0002	Free stream total temperature, cold flow
P00c	0.0121	0.0122	0.0123	0.0124	0.0125	0.0125	0.0004	Free stream static pressure, cold flow
Ptv	-0.0167	-0.0165	-0.0163	-0.0161	-0.0156	-0.0156	0.0011	Airflow Venturi total pressure
Ttv	0.0080	0.0081	0.0081	0.0081	0.0082	0.0082	0.0002	Airflow Venturi total temperature
Dth	-0.0344	-0.0334	-0.0326	-0.0322	-0.0303	-0.0303	0.0041	Airflow Venturi throat area
Cd	-0.0167	-0.0165	-0.0163	-0.0161	-0.0156	-0.0156	0.0011	Airflow Venturi discharge coefficient
Cr	-0.0167	-0.0165	-0.0163	-0.0161	-0.0156	-0.0156	0.0011	Airflow Venturi real gas critical flow coefficient
Tt00	-0.0153	-0.0152	-0.0152	-0.0152	-0.0152	-0.0152	0.0000	Free stream total pressure, hot flow
Pt00	-0.1378	-0.1376	-0.1374	-0.1373	-0.1368	-0.1368	0.0010	Free stream total temperature, hot flow
P00	-0.0455	-0.0452	-0.0449	-0.0448	-0.0441	-0.0441	0.0014	Free stream static pressure, hot flow
Kfactor	1.0000	1.0000	1.0000	1.0000	1.0000	1.0000	0.0000	Fuel flowmeter calibration table
Top	0.2519	0.2523	0.2527	0.2529	0.2537	0.2537	0.0018	Fuel temperature at flowmeter
Tcal	0.0150	0.0150	0.0150	0.0150	0.0150	0.0150	0.0000	Fuel temperature during flowmeter calibration
SG60f	-1.0138	-1.0087	-1.0046	-1.0026	-0.9937	-0.9937	0.0202	Specific gravity of fuel at 60°F
Freq	-1.0099	-1.0048	-1.0008	-0.9988	-0.9899	-0.9899	0.0200	Fuel flowmeter frequency
A5	-0.1594	-0.1591	-0.1589	-0.1588	-0.1583	-0.1583	0.0011	Nozzle throat area
Cdn	0.1599	0.1594	0.1590	0.1588	0.1578	0.1578	0.0021	Nozzle discharge coefficient
Pamb	-0.2642	-0.2639	-0.2637	-0.2636	-0.2631	-0.2631	0.0011	Ambient pressure
A6	-0.2702	-0.2702	-0.2702	-0.2702	-0.2702	-0.2702	0.0000	Nozzle exit area
Fm	-1.7121	-1.7121	-1.7121	-1.7121	-1.7121	-1.7121	0.0000	Measured scale force, hot flow
Pneb	-0.0796	-0.0796	-0.0796	-0.0796	-0.0796	-0.0796	0.0000	Nozzle exit base pressure, hot flow
Ppb	0.1115	0.1115	0.1115	0.1115	0.1115	0.1115	0.0000	Pylon base pressure, hot flow
Fmc	3.1303	3.1303	3.1303	3.1303	3.1303	3.1303	0.0000	Measured scale force, cold flow
Fnc	-0.4453	-0.4453	-0.4453	-0.4453	-0.4453	-0.4453	0.0000	net thrust, cold flow
Pnebc	0.0908	0.0908	0.0908	0.0908	0.0908	0.0908	0.0000	Nozzle exit base pressure, cold flow
Aneb	0.0111	0.0111	0.0111	0.0111	0.0111	0.0111	0.0000	Nozzle exit base area
Ppbc	-0.0955	-0.0955	-0.0955	-0.0955	-0.0955	-0.0955	0.0000	Pylon base pressure, cold flow
Apb	0.0159	0.0159	0.0159	0.0159	0.0159	0.0159	0.0000	Pylon base area
etan	2.4764	2.4764	2.4764	2.4764	2.4764	2.4764	0.0000	Nozzle stream thrust efficiency

VITA

Kevin Raymond Holst was born in Fort Belvoir, VA in October 1983 to Mr. Herbert Holst and Mrs. Susan Holst. He and his family moved to Bartlett, Tennessee in 1988 after a brief stay in Belleville, Illinois. He attended Altruria Elementary, Elmore Park Middle, and Bartlett High schools in Bartlett, Tennessee. In 2002 he graduated from Bartlett High School and enrolled at Middle Tennessee State University to become a professional pilot. After some discussion with his advisor, he realized that engineering may be a better fit for him, and in the spring semester of 2005 he transferred to the University of Tennessee at Knoxville to study Aerospace Engineering. He graduated Summa Cum Laude from the University of Tennessee at Knoxville in May 2007 and began working for Aerospace Testing Alliance at Arnold Engineering Development Complex that July. Kevin remains working at AEDC and resides in Murfreesboro, Tennessee with his wife, Kimberly, and two dogs, Peyton and Birdie.